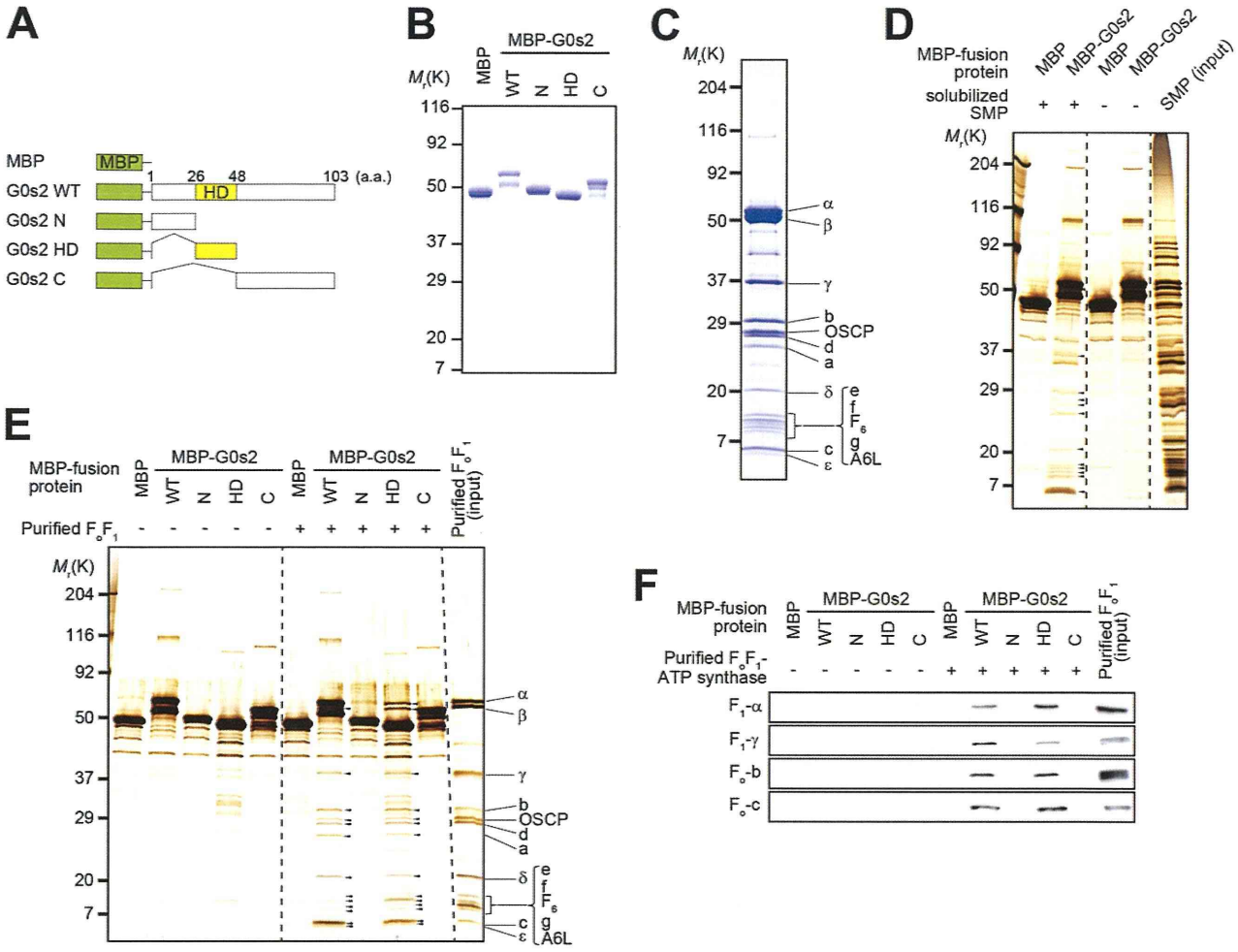

Fig. S5. G0s2 directly interacts with F_oF_1-ATP synthase. (*A*) A schematic representation of recombinant maltose-binding protein (MBP)-fusion proteins purified from *Escherichia coli*. (*B*) Coomassie Brilliant Blue-stained gel of recombinant MBP-fusion proteins purified from *E. coli*. (*C*) Coomassie Brilliant Blue-stained gel of purified F_oF_1-ATP synthase from bovine heart mitochondria. OSCP, oligomycin sensitivity conferral protein. (*D* and *E*) A silver-stained gel of an in vitro pull-down assay using (*D*) submitochondrial particles (SMPs) or (*E*) purified F_oF_1-ATP synthase from bovine heart mitochondria. Arrowheads indicate the F_oF_1-ATP synthase subunits bound to G0s2 protein. (*F*) Immunoblotting of an in vitro pull-down assay using purified F_oF_1-ATP synthase.

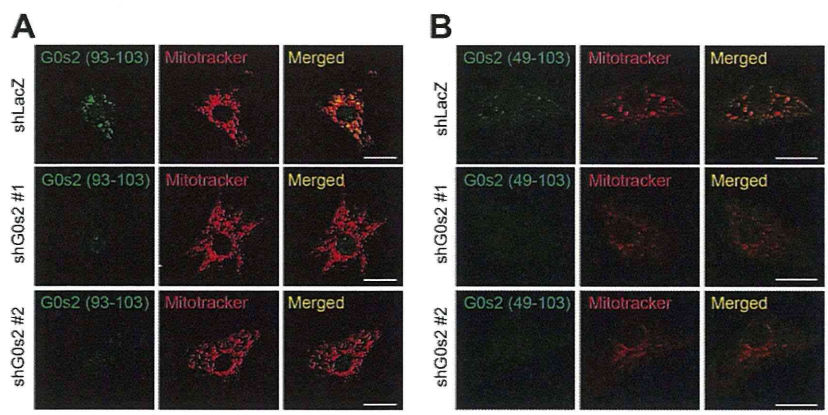

Fig. S6. G0s2 is localized to mitochondria. Immunostaining with an antibody against mouse (*A*) G0s2 (93–103 aa) or (*B*) G0s2 (49–103 aa) in cardiomyocytes expressing shLacZ, shG0s2 #1, and shG0s2 #2. (Scale bars: 20 μm.)

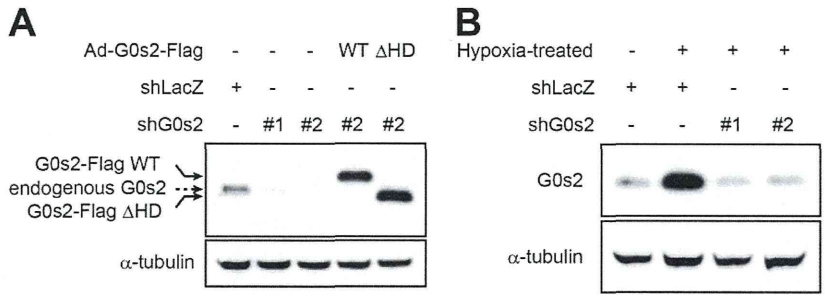

Fig. S7. (*A*) Immunoblotting of G0s2-depleted cardiomyocytes rescued by overexpression of G0s2-Flag. (*B*) Immunoblotting of G0s2-depleted cardiomyocytes under hypoxic conditions. Cardiomyocytes expressing the indicated adenovirus were exposed to hypoxia (1% O_2) for 4 h. The cell lysates were subjected to immunoblotting with anti-G0s2 or α-tubulin antibodies.

Table S1. The identification of proteins that specifically bound to G0s2 by MS

SwissProt accession	Description	Molecular mass (Da)	PLGS score	Peptides	Coverage (%)
ATPA_RAT	ATP synthase subunit-α mitochondrial	59,716	10.5798	10	18.9873
ATPB_RAT	ATP synthase subunit-β mitochondrial	56,318	10.5798	11	24.1966
ATPG_RAT	ATP synthase γ-chain	32,975	10.523	2	7.3826
ATP5F1_RAT	ATP synthase subunit b mitochondrial	28,850	10.5796	2	3.9063
ATPO_RAT	ATP synthase subunit O mitochondrial	23,382	10.5796	5	23.9437
ATP5H_RAT	ATP synthase subunit d mitochondrial	18,751	10.5796	2	13.0435
ATPD_RAT	ATP synthase subunit-δ mitochondrial	17,584	10.5796	2	13.6905
D3ZAF6_RAT	ATP synthase H transporting mitochondrial Fo complex subunit f isoform 2	10,972	10.5796	2	22.3404

A PLGS score was calculated by the Protein Lynx Global Server (PLGS; PLGS 2.4) software using a Monte Carlo algorithm to analyze all of the available MS data; this score is a statistical measure of the accuracy of assignation. A higher score implies a greater confidence in the identity of the protein.

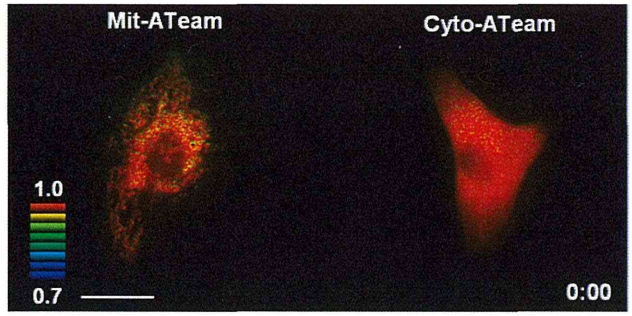

Movie S1. Time-lapse imaging of the (*Left*) Mit-ATeam and (*Right*) Cyto-ATeam fluorescence in cardiomyocytes before and after the addition of oxidative phosphorylation inhibitor. YFP/CFP ratiometric pseudocolored images were obtained every 1 min for 25 min. Oligomycin A (0.01 μg/mL), an inhibitor of F_oF_1-ATP synthase, was added at time point 5 min. (Scale bar: 20 μm.)

Movie S1

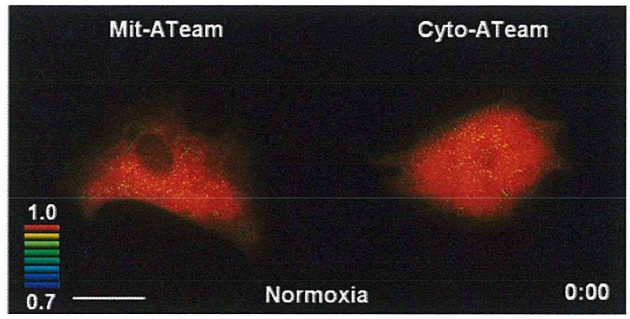

Movie S2. Time-lapse imaging of the (*Left*) Mit-ATeam and (*Right*) Cyto-ATeam fluorescence in cardiomyocytes exposed to hypoxia. YFP/CFP ratiometric pseudocolored images were obtained every 30 min for 3 h. Cells are exposed to 1% hypoxia from the time point 30 min. (Scale bar: 20 μm.)

Movie S2

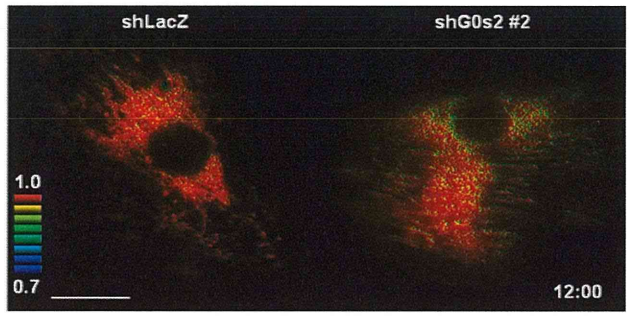

Movie S3. Time-lapse imaging of the Mit-ATeam fluorescence in cardiomyocytes that expressed (*Left*) shLacZ or (*Right*) shG0s2 #2. YFP/CFP ratiometric pseudocolored images were obtained every 1 h for 12 h. An inhibitor of F_oF_1-ATP synthase (1 μg/mL oligomycin A) was added at the end of time-lapse imaging to completely inhibit ATP synthesis. (Scale bar: 20 μm.) The indicated times designate the periods after adenovirus infection.

Movie S3

Movie S4. Time-lapse imaging of the Cyto-ATeam fluorescence in cardiomyocytes that expressed (*Left*) shLacZ or (*Right*) shG0s2 #2. YFP/CFP ratiometric pseudocolored images were obtained every 1 h for 12 h. Inhibitors of both glycolysis (10 mM 2-deoxyglucose) and F_oF_1-ATP synthase (1 μg/mL oligomycin A) were added at the end of the time-lapse imaging to decrease the cytosolic ATP concentration. (Scale bar: 20 μm.) The indicated times designate the periods after adenovirus infection.

Movie S4

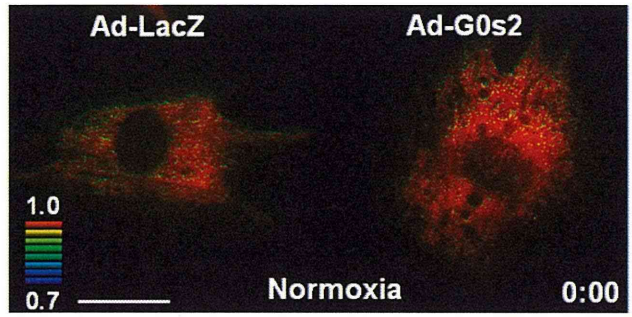

Movie S5. Time-lapse imaging of the Mit-ATeam fluorescence in cardiomyocytes that expressed (*Left*) LacZ or (*Right*) G0s2 during hypoxia and reoxygenation. YFP/CFP ratiometric pseudocolored images were obtained every 30 min for 4 h. The cells were exposed and imaged under hypoxic condition from the time point 30 min to 4 h. (Scale bar: 20 μm.)

Movie S5

The FASEB Journal • Research Communication

Noninvasive and quantitative live imaging reveals a potential stress-responsive enhancer in the failing heart

Ken Matsuoka,[*,†] Yoshihiro Asano,[*,†,1] Shuichiro Higo,[*,†] Osamu Tsukamoto,[†] Yi Yan,[†] Satoru Yamazaki,[§] Takashi Matsuzaki,[*] Hidetaka Kioka,[*,†] Hisakazu Kato,[†] Yoshihiro Uno,[‡] Masanori Asakura,[‖] Hiroshi Asanuma,[¶] Tetsuo Minamino,[*] Hiroyuki Aburatani,[#] Masafumi Kitakaze,[‖] Issei Komuro,[*] and Seiji Takashima[*,†]

[*]Department of Cardiovascular Medicine and [†]Department of Medical Biochemistry and [‡]Laboratory of Reproductive Engineering, Institute of Experimental Animal Sciences, Osaka University Graduate School of Medicine, Suita, Japan; [§]Department of Cell Biology and [‖]Department of Clinical Research and Development, National Cerebral and Cardiovascular Center Research Institute, Suita, Japan; [¶]Department of Cardiovascular Science and Technology, Kyoto Prefectural University School of Medicine, Kyoto, Japan; and [#]Genome Science Division, Research Center for Advanced Science and Technology, University of Tokyo, Tokyo, Japan

ABSTRACT **Recent advances in genome analysis have enabled the identification of numerous distal enhancers that regulate gene expression in various conditions. However, the enhancers involved in pathological conditions are largely unknown because of the lack of *in vivo* quantitative assessment of enhancer activity in live animals. Here, we established a noninvasive and quantitative live imaging system for monitoring transcriptional activity and identified a novel stress-responsive enhancer of *Nppa* and *Nppb*, the most common markers of heart failure. The enhancer is a 650-bp fragment within 50 kb of the *Nppa* and *Nppb* loci. A chromosome conformation capture (3C) assay revealed that this distal enhancer directly interacts with the 5′-flanking regions of *Nppa* and *Nppb*. To monitor the enhancer activity in a live heart, we established an imaging system using the firefly luciferase reporter. Using this imaging system, we observed that the novel enhancer activated the reporter gene in pressure overload-induced failing hearts (failing hearts: 5.7±1.3-fold; sham-surgery hearts: 1.0±0.2-fold; $P<0.001$, repeated-measures ANOVA). This method will be particularly useful for identifying enhancers that function only during pathological conditions.—Matsuoka, K., Asano, Y., Higo, S., Tsukamoto, O., Yan, Y., Yamazaki, S., Matsuzaki, T., Kioka, H., Kato, H., Uno, Y., Asakura, M., Asanuma, H., Minamino, T., Aburatani, H., Kitakaze, M., Komuro, I., and Takashima, S. Noninvasive and quantitative live imaging reveals a potential stress-responsive enhancer in the failing heart. *FASEB J.* 28, 1870–1879 (2014). www.fasebj.org**

Key Words: natriuretic peptide · transcriptional regulation · in vivo *assessment*

GENE EXPRESSION IS REGULATED through the integrated action of many *cis*-regulatory elements, including core promoters, proximal promoters, distant enhancers, and insulators (1). Several methods have been used to explore the function of *cis*-regulatory elements during a variety of developmental stages (2, 3). However, the identification of gene regulatory elements with pathophysiological roles has been technically difficult because there are few appropriate models for monitoring transcriptional activity in live animals under pathological conditions.

Here, we focused on the regulatory elements that are responsive to heart failure. The natriuretic peptides, atrial natriuretic peptide (ANP) and brain natriuretic peptide (BNP), encoded by the neighboring genes *Nppa* and *Nppb* are activated in the embryonic heart, down-regulated after birth, and then reactivated during heart failure. Both peptides are well-known biomarkers that are strongly induced during heart failure and represent its severity. Cardiologists frequently use these peptides as natriuretic and vasorelaxant agents to treat various clinical conditions (4–8). Many studies have tried to elucidate the mechanisms of their transcriptional regulation because factors that regulate these

Abbreviations: 3C, chromosome conformation capture; ANP, atrial natriuretic peptide; BNP, brain natriuretic peptide; ChIP-seq, chromatin immunoprecipitation sequencing; CMV, cytomegalovirus; CR, conserved region; CTCF, CCCTC-binding factor; H3K4me1, histone H3 monomethylated at lysine 4; H3K4me3, histone H3 trimethylated at lysine 4; PE, phenylephrine; TAC, transverse aortic constriction

[1] Correspondence: Osaka University Graduate School of Medicine, 2-2 Yamadaoka, Suita, Osaka 565–0871, Japan. E-mail: asano@cardiology.med.osaka-u.ac.jp

doi: 10.1096/fj.13-245522

This article includes supplemental data. Please visit *http://www.fasebj.org* to obtain this information.

natriuretic peptides are potential therapeutic targets for heart disease (9–14).

Mice transgenic for various loci, including the 5′-flanking regions of the natriuretic peptide genes, have been used to identify the regulatory elements required for transcriptional activation either during heart development or in the diseased heart. These studies reported that the 5′-flanking regions of the natriuretic peptide genes regulated their expression during heart development (9, 10, 13); however, the 5′-flanking regions were not responsible for their specific reactivation in the diseased heart (11, 12). A recent study identified the distal enhancer elements regulating the natriuretic peptide genes in the developing heart by examining cardiac-specific transcription factor binding sites; however, these enhancer elements did not respond to heart failure (14). Therefore, the stress-responsive regulatory elements that function during heart failure have not yet been identified and are potentially located outside the 5′-flanking regions.

In this study, we aimed to identify the novel stress-responsive enhancer elements of the *Nppa* and *Nppb* genes in the failing heart. Furthermore, we established a noninvasive and quantitative live imaging assay to monitor the transcriptional activity of candidate enhancers in the failing heart. *In vivo* live imaging of the firefly luciferase reporter in a single mouse enabled us to analyze the sequential changes in enhancer activity during the progression of heart failure. Combined with a fine mapping technique using epigenetic markers, we identified a 650-bp stress-responsive enhancer that was strongly activated by cardiac hypertrophy and heart failure.

MATERIALS AND METHODS

Animals

All procedures were performed according to the U.S. National Institutes of Health (NIH) Guide for the Care and Use of Laboratory Animals (NIH publication no. 85-23, revised 1996) and were approved by the Animal Experiments Committee, Osaka University (approval no. 21-78-10).

Reagents and antibodies

Phenylephrine (PE) was purchased from Sigma-Aldrich (St. Louis, MO, USA). The anti-RNA polymerase II and anti-histone H3 trimethylated at lysine 4 (H3K4me3) antibodies used for chromatin immunoprecipitation sequencing (ChIP-seq) were kind gifts from Dr. H. Kimura (Graduate School of Frontier Biosciences, Osaka University).

Primary culture of neonatal rat cardiomyocytes

Ventricular myocytes obtained from 1- or 2-d-old Wistar rats were prepared and cultured overnight in Dulbecco's modified Eagle's medium (Sigma-Aldrich) containing 10% FBS, as described previously (15).

Comparative genomics

Genome-wide multiple alignments of the genomic sequences containing the *Nppa* and *Nppb* genes were performed using the University of California Santa Cruz (UCSC) Genome Browser (16); 8 vertebrate species were compared, including mouse (mm9, July 2007), rat (m4, Nov. 2004), human (hg18, Mar. 2006), orangutan (ponAbe2, July 2007), dog (canFam2, May 2005), horse (equCab1, Jan. 2007), opossum (monDom4, Jan. 2006), and chicken (galGal3, May 2006). We used vertebrate Multiz alignment of DNA sequences (17) to analyze the homology of DNA sequences among mouse and other species. We used the Placental Mammal Basewise Conservation assessed by PhyloP (18) to assess the degree of mammalian conservation. Next, we identified discrete conserved fragments. The transcribed sequences within the conserved set were filtered out using known genes, spliced ESTs, and mRNA annotations obtained from the UCSC genome browser. Finally, we manually curated the data set to remove any additional false positives by visual examination of the UCSC genomic data. We defined the noncoding conserved regions (CRs) that were homologous at least in the human and mouse genomes and at least 1 kb away from the transcription start sites as the enhancer candidates.

ChIP sequencing on mouse heart tissues

Whole hearts were isolated from 8-wk-old C57BL6 mice, perfused rapidly with cold PBS, flash-frozen in liquid nitrogen, homogenized using a sterile tissue grinder, and cross-linked with 0.3% paraformaldehyde. Subsequently, chromatin isolation, sonication, and immunoprecipitation using an anti-RNA polymerase II antibody and an anti-H3K4me3 antibody were performed. The ChIP DNA and input samples were sheared by sonication, end-repaired, ligated to the sequencing adapters, and amplified. The purified ChIP DNA library samples were sequenced using the Illumina Genome Analyzer II (Illumina, Inc., San Diego, CA, USA). Unfiltered sequence reads were aligned to the mouse reference genome [U.S. National Center for Biotechnology Information (NCBI) build 37, mm9] using Bowtie. RNA polymerase II- and H3K4me3-enriched regions were identified using MACS (19) with the default parameters.

Lentiviral enhancer assay

Eleven CRs were PCR amplified from the mouse BAC clone containing the *Nppa* and *Nppb* loci (clone RP23-128E8; BACPAC Resources Center, Children's Hospital Oakland, Oakland, CA, USA; primers and probes are listed in Supplemental Table S1). The PCR fragments were subcloned into the pCR-Blunt II-TOPO vector (Invitrogen, Carlsbad, CA, USA) and recombined into a lentiviral vector encoding the firefly luciferase reporter (pGreenFire Transcriptional Reporter Lentivector; System Biosciences, Mountain View, CA, USA). The lentiviral particles were produced by transfection of 293T cells with the 3 lentiviral packaging plasmids (*i.e.*, pMDLg/pRRE, pRSV-Rev, and pMD2.VSV.G) using Lipofectamine 2000 (Invitrogen). The supernatant from 293T cells containing the lentiviral particles was collected 48 h after transfection, sterilized using a 0.45-μm cellulose acetate filter, and concentrated by centrifugation (Peg-it Virus Precipitation Solution, System Biosciences).

Rat neonatal cardiomyocytes isolated as described above were plated in 96-well plates. The next day, the medium was replaced with a serum-free medium containing the lentiviral vector, and the cells were incubated for 12 h. Subsequently, the cardiomyocytes were exposed to 100 μM PE for 48 h prior to the luciferase assay.

RNA extraction and quantitative RT-PCR

The total RNA was prepared from rat cardiomyocytes, rat cardiac fibroblasts, murine hearts, and murine brains using the RNA-Bee RNA isolation reagent (Tel-Test, Friendswood, TX, USA) and then converted to cDNA using the high-capacity cDNA reverse transcription kit (Applied Biosystems, Foster City, CA, USA), according to the manufacturer's instructions. The quantitative RT-PCR was performed using the TaqMan technology and the StepOnePlus real-time PCR System (Applied Biosystems). All samples were processed in duplicate. The level of each transcript was quantified according to the threshold cycle (C_t) method using GAPDH as an internal control. Inventoried TaqMan gene expression assays were used: *Nppa*, Rn0056661, Mm01255748; *Nppb*, Rn00580641, Mm01255770; *Gapdh*, rodent GAPDH control reagent.

3C analysis

The whole hearts of the mice were isolated, perfused rapidly with cold PBS, flash-frozen in liquid nitrogen, homogenized using a sterile tissue grinder, and fixed with 1% paraformaldehyde. The cross-linked tissues utilized for 3C experiments were subjected to digestion with *Bam*HI following standard protocols (20, 21). The mouse BAC DNA containing *Nppa* and *Nppb* (clone RP23-128E8) was used as a control. The TaqMan real-time PCR was performed using probes near the restriction sites; the primers and probes are listed in Supplemental Table S2.

Transgenic mouse enhancer assay

The candidate enhancer regions were cloned into a vector encoding the minimal CMV promoter driving the luciferase gene as described above. Transgenic mouse embryos were generated by pronuclear injection into the zygotes of BDF1 mice using standard methods. Because black fur attenuates light transmission, albino mice were generated by crossing the transgenic founders to ICR albino mice.

In vivo bioluminescence imaging

Prior to *in vivo* imaging, the mice were anesthetized using isoflurane, and the black mice were shaved from the neck to the lower torso to allow the optimal visualization of fluorescence without interference from the black fur. A D-luciferin solution was injected intraperitoneally (150 mg/kg i.p.) or intravenously (75 mg/kg i.v.). The mice were imaged using an *in vivo* live imaging system (IVIS Lumina II; Caliper Life Sciences, Waltham, MA, USA). For quantification, the bioluminescence light intensity was measured at the region of interest and expressed in relative light units (RLU/min) using Living Image 4.0 (Caliper Life Sciences). To calculate the enhancer activity in the heart, we defined the ratio of heart to brain luciferase intensities as the cardiac-specific enhancer activity.

Transverse aortic constriction (TAC)

Transgenic mice aged 8 wk and weighing 20–25 g were subjected to pressure overload, as described previously (22). Briefly, the chest was entered *via* the second intercostal space at the upper left sternal border. After the arch of the aorta was isolated, a TAC was created using a 7-0 suture tied twice around a 27-gauge needle and the aortic arch, between the innominate and left common carotid arteries. After the suture was tied, the needle was gently removed, yielding 60–80% constriction of the aorta.

PE-induced hypertrophy

Transgenic mice aged 8 wk and weighing 20–25 g were treated with PE (75 mg/kg/d) using an osmotic minipump (Alzet, Cupertino, CA, USA) to induce cardiac hypertrophy, as previously reported (23, 24).

Statistical analysis

Data are expressed as means ± SE. The 2-tailed Student's *t* test and repeated ANOVA were used to analyze differences between the groups. Values of $P < 0.05$ were considered to represent a significant difference.

RESULTS

Identification of candidate enhancers near the *Nppa-Nppb* locus using comparative genomics and ChIP-seq

To identify potential enhancers, we performed a comparative analysis of the genomic sequences of mouse and divergent species and identified CRs that may function as common regulatory sequences (25–27). We defined CRs that were homologous at least in the human and mouse genomes and at least 1 kb away from the transcription start sites of *Nppa* and *Nppb* as the candidate enhancers. First, we analyzed the 50-kb *Nppa-Nppb* locus bounded by the binding sites of 2 CCCTC-binding factors (CTCFs), which can function as insulators (28, 29). Using a genome database (30), we identified 11 CRs, including the *Nppa* and *Nppb* introns in the 50-kb region (**Fig. 1**).

Next, we performed a ChIP-seq analysis on RNA polymerase II and H3K4me3 in the adult mouse heart. We analyzed the epigenetic modifications near the *Nppa* and *Nppb* genes combined with the ChIP-seq analysis using a public database of the adult mouse heart (30). We hypothesized that the normal heart would have activated epigenetic marks because *Nppa* and *Nppb* are expressed, albeit at low levels, in normal conditions. Recent genome-wide studies have determined that enhancers can be defined as DNA sequences bound by the RNA polymerase II and transcriptional coactivator protein p300, and where histone H3 monomethylated at lysine 4 (H3K4me1) accumulates instead of H3K4me3 (31–34). Among the 11 CRs identified, only CR9 coincided with the binding sites of RNA polymerase II and p300, and overlapped with the gene areas modified by H3K4me1, and filled all criteria for the enhancer (Fig. 1). In addition, H3K4me1 modifications in CR9 were only observed in the heart but not in the other organs (Fig. 1 and Supplemental Fig. S1). Therefore, we analyzed the 11 CRs, including CR9, as the most likely distal candidate enhancers for the stress-responsive regulatory regions of the natriuretic peptide genes.

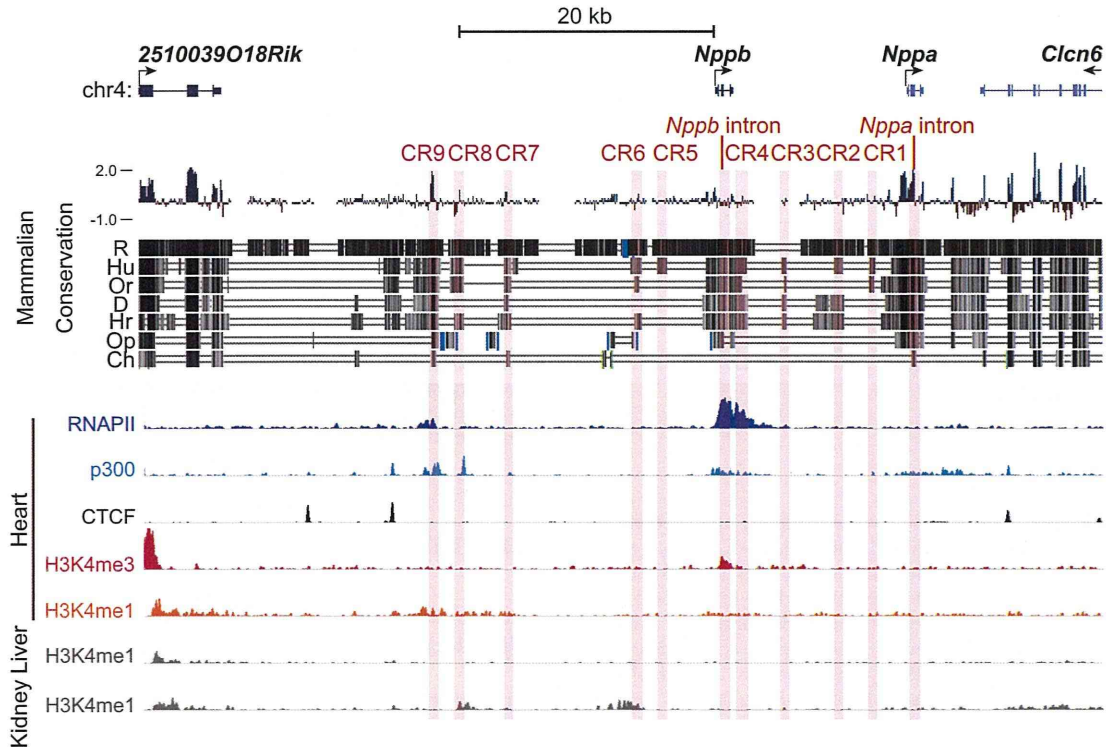

Figure 1. Mammalian evolutionarily conserved regions and ChIP-seq data surrounding the murine *Nppa* and *Nppb* loci. We used an open database on the University of California Santa Cruz (UCSC) Genome Browser to assess the degree of DNA sequence conservation around *Nppa* and *Nppb* gene loci. Blue and red vertical lines, the Placental Mammal Basewise Conservation assessed by PhyloP; black vertical lines, the vertebrate Multiz alignment of DNA sequences among mice and 7 other species (rats, humans, orangutans, dogs, horses, opossums, and chickens). We defined noncoding conserved regions (CRs) that were homologous at least in the human and mouse genomes and at least 1 kb away from the transcription start sites of *Nppa* and *Nppb* as the candidate enhancers. CRs are highlighted as light red vertical bars (CR1-9, *Nppa* intron, and *Nppb* intron). ChIP-seq data for H3K4me1, p300, and CTCF were obtained from an open database of the adult mouse heart. Some CRs coincided with the peaks for H3K4me1, RNA polymerase II, and the transcriptional coactivator protein p300. R, rat; Hu, human; Or, orangutan; D, dog; Hr, horse; Op, opossum; Ch, chicken.

Identification of a distal enhancer element responsive to an α_1-adrenergic receptor agonist

We screened the candidate enhancers for potential stress-responsive regulatory regions. We analyzed the enhancer activity of these 11 CRs after treatment with PE, an α_1-adrenergic receptor agonist, which mimics cardiac overload and induces *Nppa* and *Nppb* expression in cardiomyocytes (35). We confirmed that PE induced the expression of endogenous *Nppa* and *Nppb* specifically in cardiomyocytes but not in cardiac fibroblasts (**Fig. 2*A***). Then, we introduced the 11 CRs with a minimum human cytomegalovirus (CMV) promoter and the luciferase gene into rat cardiomyocytes using a lentiviral vector system.

Among the 11 CRs tested, only CR9, which is located 22 kb upstream from the *Nppb* transcription start site and shows high mammalian conservation score in the Placental Mammal Basewise Conservation by PhyloP (Fig. 2*B*), reproducibly increased the PE-induced luciferase activity by ~5-fold compared to the minimal CMV promoter alone (Fig. 2*C*). However, CR9 did not respond to PE in cardiac fibroblasts (Fig. 2*C*). These results suggest that CR9 is the regulatory element that is responsive to PE specifically in cardiomyocytes.

Long-range physical interaction between the distal enhancer element and the proximal promoters of the *Nppa* and *Nppb* genes

Confirming the looping interactions between distal elements and promoters is one way to demonstrate the transcriptional regulatory activity of distal elements. We performed a 3C assay (20) to comprehensively investigate whether the genomic region containing CR9 moved closer to the *Nppa* or *Nppb* promoter in an adult murine heart treated with a continuous infusion of PE *in vivo*.

The ligation frequencies were quantified by TaqMan real-time PCR using specific primers and probes and were compared to the ligation frequency of noncross-linked *Bam*HI-digested BAC DNA containing the *Nppa-Nppb* locus. We observed that CR9 interacts with both the *Nppa* and *Nppb* promoter regions at a higher frequency relative to other gene areas (Fig. 2*D*); furthermore, PE treatment strengthened these interac-

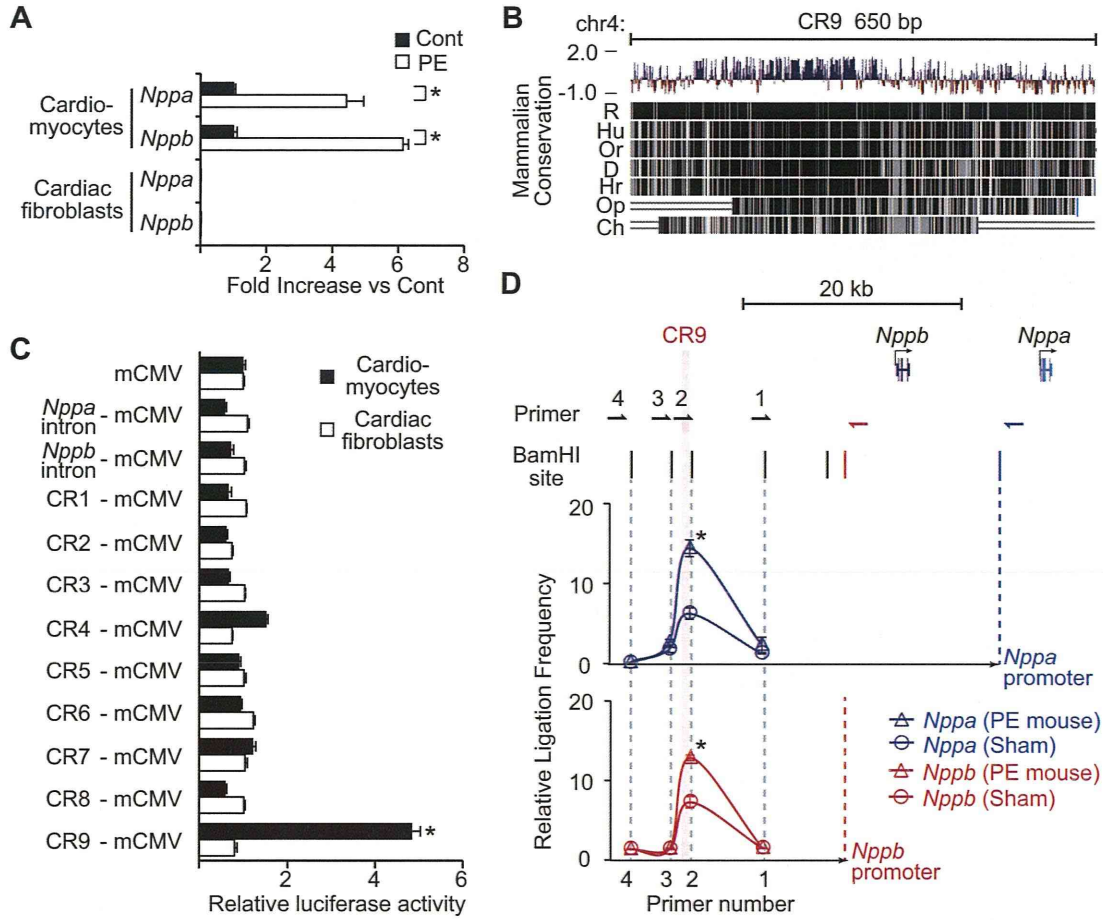

Figure 2. Identification of a distal enhancer element that is responsive to an α_1-adrenergic receptor agonist. *A*) Relative transcript levels of *Nppa* and *Nppb* in rat neonatal cardiomyocytes and cardiac fibroblasts 48 h after treatment with PE (100 μM). Values are means ± SE (n=3 cultures). *$P < 0.01$ *vs.* control; *t* test. *B*) CR9 is a highly conserved genomic region in vertebrates. *C*) Relative luciferase reporter activities of CRs in rat neonatal cardiomyocytes and cardiac fibroblasts 48 h after treatment with PE (100 μM). PE-induced luciferase activity driven by the mCMV promoter was defined as 1. Values are means ± SE (n=5 cultures). *$P < 0.001$ *vs.* mCMV alone; *t* test. *D*) *In vivo* 3C analysis of the murine *Nppa* and *Nppb* loci, showing relative ligation frequencies of each primer to the *Nppa* promoter (blue triangle, mouse with PE treatment; blue circle, mouse without PE) and the *Nppb* promoter (red triangle, mouse with PE treatment; red circle, mouse without PE). Vertical bars and arrows show the positions of *Bam*HI sites and primers. Data were normalized to the amplification value of a *Bam*HI-digested and religated BAC clone, which included the *Nppa* and *Nppb* loci (means ± SE; n=2 hearts). R, rat; Hu, human; Or, orangutan; D, dog; Hr, horse; Op, opossum; Ch, chicken. *$P < 0.05$ *vs.* control; *t* test.

tions (Fig. 2*D*). These results suggest that there is a close proximity between the distal genomic region containing CR9 and the proximal promoters of the *Nppa* and *Nppb* genes in the PE-induced hypertrophic heart.

Establishment of an *in vivo* live imaging system for gene expression in a murine model of heart disease

We confirmed the activity of the newly identified enhancer CR9 in the heart *in vivo*. The conventional histological evaluation of LacZ reporter expression in the heart only provides data at a single time point; therefore, this method cannot be employed for kinetic assessments or time course analyses of reporter expression in a live heart.

To overcome this difficulty, we established a noninvasive and quantitative live imaging system that allowed real-time monitoring of the firefly luciferase reporter. We generated 3 transgenic mouse lines (Tg-line1, Tg-line2, and Tg-line3) in which the CR9 enhancer element and a minimal CMV promoter driving the luciferase reporter gene were introduced into the germline. The live-imaging system detected luciferase expression in the heart, brain, and intestine of the Tg-line1 (**Fig. 3*A***), in the heart, salivary glands, and skin of the Tg-line2 (Supplemental Fig. S2*A*), and in the heart of the Tg-line3 (Supplemental Fig. S2*E*).

To identify the organs in which CR9 functioned as a stress-responsive enhancer, we examined the luciferase reporter expression in each organ by quantitative PCR. Continuous infusion of PE increased the blood pressure and resulted in cardiac hypertrophy (24, 36). The

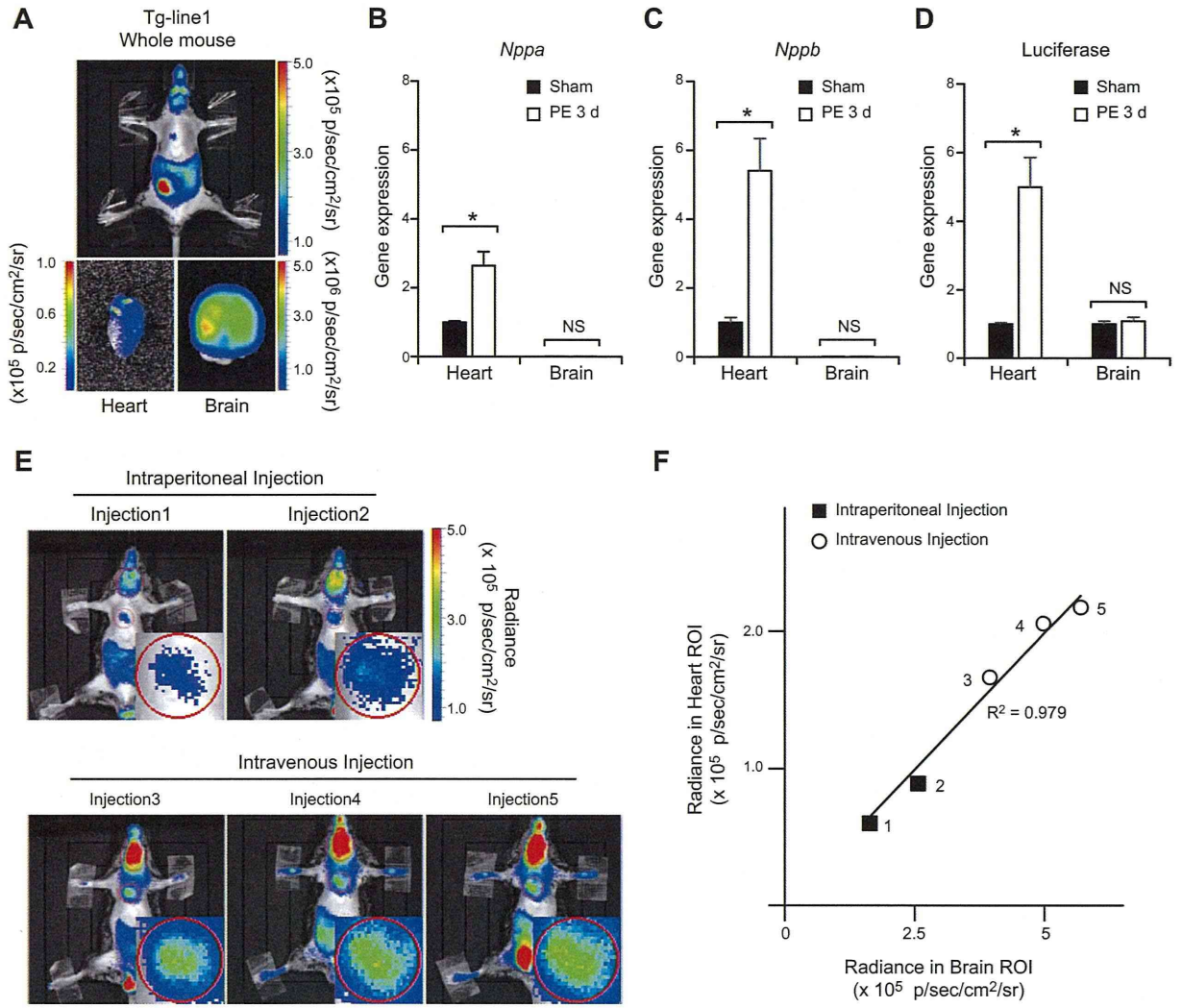

Figure 3. Establishment of an *in vivo* live imaging system for enhancer activity. *A*) Chemiluminescence imaging of CR9 in a mouse of Tg-line1. Top panel: result from whole-animal *in vivo* live imaging. Bottom panels: chemiluminescence images of the heart and brain in the same mouse. *B, C*) Relative transcript levels of *Nppa* and *Nppb* in the ventricular myocardium and brain of CR9 Tg-line1 mice treated with continuous infusion of PE for 3 d. Average transcript level in the ventricular myocardium of preinfused mice was defined as 1 (means ± SE; n=5 hearts). *$P < 0.01$ *vs.* sham-infused mice; *t* test. *D*) Relative transcript levels of luciferase reporter in the ventricular myocardium and brain of the CR9 Tg-line1 mice continuously infused with PE for 3 d. Average transcript level in the ventricular myocardium and brain of preinfused mice was defined as 1. (means ± SE; n=5 hearts). *$P < 0.01$ *vs.* sham-infused mice; *t* test. *E*) Comparison of the chemiluminescence intensities obtained using different luciferin injection methods in a Tg-line1 mouse; injections 1 and 2, intraperitoneal injections (top panels), injections 3, 4, and 5, intravenous injections (bottom panels). Injections were performed ≥4 h apart to eliminate the effect of the previous injection. Inset in each panel shows a magnified image of the heart. *F*) Scatterplots of the chemiluminescence intensities in the heart and brain. Plots indicate the independent experiments shown in each panel in *E*. There is a linear relationship between the expression in the heart and the brain, $R^2 = 0.979$.

expression of endogenous *Nppa* and *Nppb* mRNA increased 3 d after the PE infusion began (Fig. 3*B, C* and Supplemental Fig. S2*B, C, F, G*). Concomitantly, the quantitative PCR analysis of the CR9 luciferase mRNA expression showed enhanced expression in the ventricular myocardium 3 d after the PE infusion (Fig. 3*D* and Supplemental Fig. S2*D, H*). On the other hand, in the brain and the salivary glands where neither *Nppa* nor *Nppb* is highly expressed, the CR9-driven luciferase mRNA expression did not respond to PE (Fig. 3*B–D* and Supplemental Fig. S2*B–D, F–H*). Therefore, the patterns of PE-induced luciferase expression suggest that CR9 is almost exclusively active in the heart. Because the integration sites were random in these three lines, the patterns of luciferase expression depend on CR9 or other enhancers near the integrated sites. The expression of luciferase in the brain of Tg-line1 and salivary glands of Tg-line2, both of which express neither *Nppa* nor *Nppb,* might be driven by other enhancers near the integrated sites.

To evaluate the accuracy and reproducibility of this method, we measured the luminescence in the heart of

a mouse from Tg-line1. In this transgenic line, the brain, intestine, and testis expressed the reporter protein due to positional effects of the insertion site and most likely not due to CR9 activity. Because the luciferase mRNA expression in the brain remained unchanged after PE treatment (Fig. 3*D*), we used the reporter activity in the brain as a control. The absolute luminescence values of the heart were affected by the injection method and the amount of luciferase substrate injected (Fig. 3*E*). However, using brain luminescence as a control, we successfully eliminated the signal variations caused by these differences. The ratio of the luminescence in the heart and brain remained constant within each mouse, independent of the injection method (Fig. 3*F*). Therefore, we defined the ratio of heart to brain luciferase intensities as the cardiac-specific enhancer activity.

Distal enhancer element was activated in the murine model of heart failure

To examine whether the CR9 enhancer was also responsible for gene expression in other pathological conditions, we subjected Tg-line1 mice to heart failure induced by TAC and compared them with sham-surgery mice. This model mimics the heart condition of patients with hypertension who suffer a continuous pressure overload on the heart. The pressure overload by TAC caused potent cardiac hypertrophy at 2 wk postsurgery and reduced cardiac contractility at 3 wk postsurgery (**Fig. 4*A*, *B***), as previously reported (22). The endogenous *Nppa* and *Nppb* expression increased severalfold in the ventricular myocardium 3 wk after the TAC surgery (Fig. 4*C*). The heart to brain luciferase intensity ratio also increased severalfold 3 wk following the TAC surgery (Fig. 4*D*, *E* and Supplemental Fig. S3). However, the heart to brain luciferase intensity ratio of sham-surgery mice did not change after the surgery (Fig. 4*D*, *E* and Supplemental Fig. S3; 3 wk after TAC surgery: 5.7±1.3 fold; 3 wk after sham surgery: 1.0±0.2 fold; $P < 0.001$, repeated ANOVA). These results suggest that CR9 increases transcriptional activity during mechanical pressure overload-induced hypertrophy and subsequent heart failure.

DISCUSSION

Here, we focused on the stress-responsive regulatory elements of *Nppa* and *Nppb* in heart failure. By screening the evolutionarily conserved and epigenetically modified regions around the *Nppa* and *Nppb* gene loci, we identified a 650-bp transcriptional enhancer that was responsive to an α_1-adrenergic receptor agonist *in vitro*. Furthermore, *in vivo* 3C analysis revealed that this distal enhancer directly interacted with the 5′-flanking regions of both *Nppa* and *Nppb*. Using *in vivo* live imaging of luciferase reporter gene expression, we observed that this 650-bp enhancer caused cardiac-specific activation of reporter gene expression during the progression of pressure overload-induced heart failure. Notably, this is the first study to provide a time series analysis for monitoring enhancer activity under pathological conditions in an individual live mouse.

Although numerous approaches have been used to explore the stress-responsive regulatory elements driving gene transcription during heart failure (11, 12, 14), these elements have not yet been identified due to the technical difficulty involved. To detect the elements that are responsive to pathological conditions such as heart failure, it is essential to confirm the activity of the responsive element using a beating heart that remains connected to the systemic cardiovascular system. Therefore, it would be beneficial to establish transgenic mouse lines carrying a reporter plasmid to assess the responsive elements driving the expression of specific genes. However, the creation of multiple stable adult mouse lines to identify these elements is time-consuming.

In this study, we utilized two improved methods for reporter analysis and successfully identified a novel potent enhancer.

First, by performing an enhancer analysis using a lentiviral vector, we accurately identified candidate enhancers in cardiomyocytes and subsequently generated transgenic reporter mice. Previous promoter analyses used electroporation or lipofection to transfect cultured cardiomyocytes with plasmids (37, 38), but the transfection efficiency of these methods in primary cardiomyocytes is too low to accurately measure reporter activity during the stress response. In this study, greater than 90% transduction efficiency of cardiomyocytes was achieved using a lentiviral vector, which enabled us to accurately identify a specific enhancer fragment. Using this method, we efficiently minimized the number of reporter plasmids to be subsequently integrated into the mouse genome to screen for potential enhancers.

Second, by sequentially measuring the enhancer activity in a single live mouse, we collected robust data to assess enhancer activity in the heart *in vivo*. LacZ is not a suitable reporter for this purpose because LacZ activity can only be assessed after animal euthanization. Therefore, we overcame this limitation using the luciferase reporter plasmid. Recent advances in high-sensitivity luminescence imaging have made it possible to evaluate enhancer-driven luciferase activity without operating on the mice. Therefore, we sequentially assessed reporter activity and hemodynamic changes in the same mouse throughout the time course of the development of heart failure. These data were highly reproducible and enabled us to identify an enhancer element that was activated by cardiac overload. Because this method can be applied to any organ, the *in vivo* luciferase reporter assay may be used for assessing the *in vivo* enhancer or promoter activities responsible for clinically important diseases. The noninvasive nature of this method also enabled us to simultaneously assess the hemodynamic and metabolic parameters *in vivo* along with reporter activity. Specifically, the Tg-line1

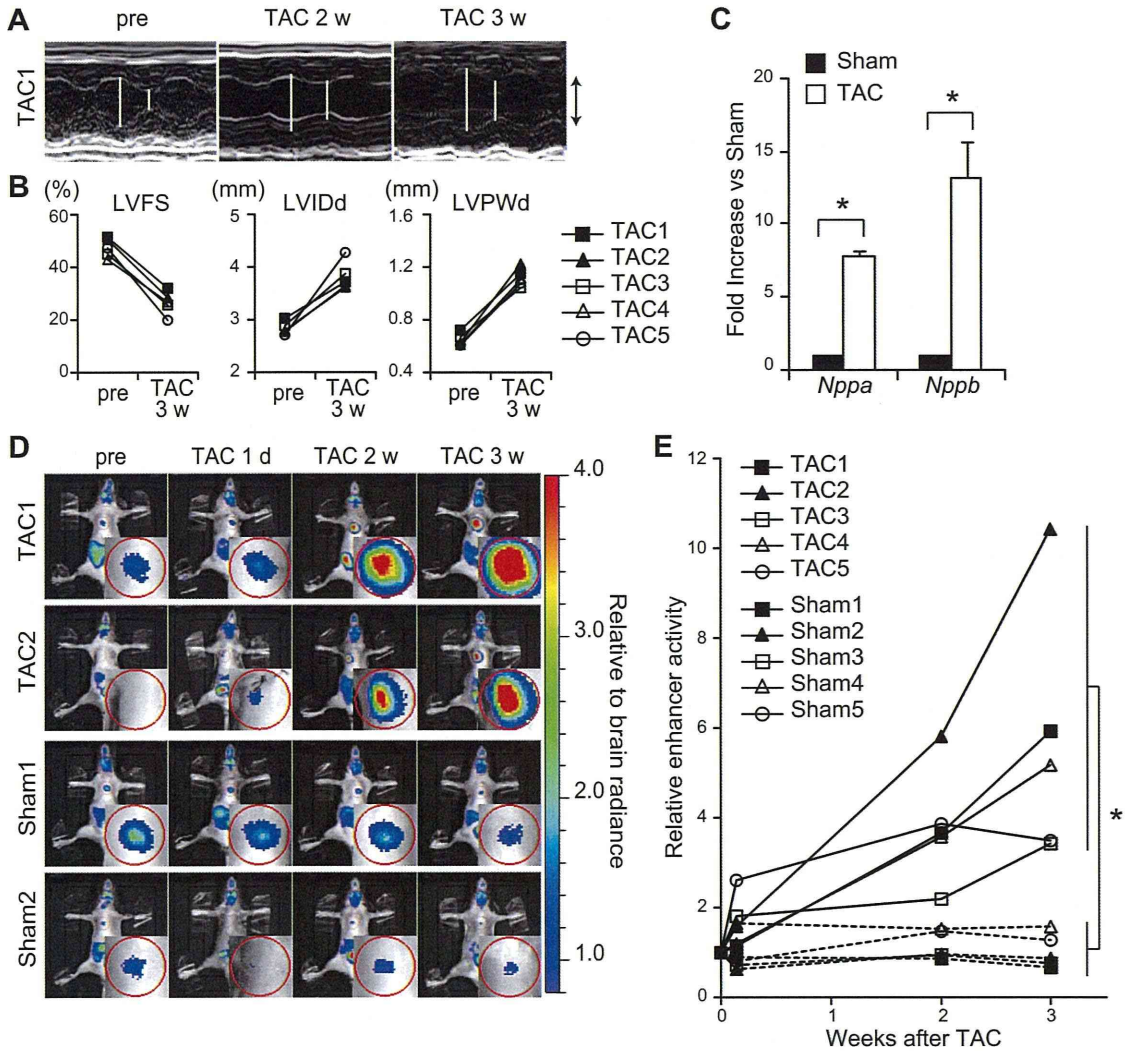

Figure 4. Distal enhancer element is reactivated in the murine model of heart failure. *A*) Representative M-mode echocardiograms in a mouse of Tg-line1 (TAC1) before and after TAC. Open bars indicate maximal left ventricular internal dimension in diastole (LVIDd) and maximal left ventricular internal dimension in systole (LVIDs). Up and down arrows represent 3 mm. *B)* Echocardiographic changes in left ventricular fractional shortening (LVFS), LVIDd, and left ventricular posterior wall thickness in diastole (LVPWd) in 5 mice of Tg-line1 (TAC1-5) before and after TAC. ***C***) Relative *Nppa* and *Nppb* transcript levels in the ventricular myocardium 3 wk after the TAC procedure (means ± SE; n=3 hearts). *$P < 0.05$ *vs.* sham-surgery mice; *t* test. *D*) Sequential *in vivo* live imaging of 4 representative Tg-line1 mice before and after TAC or sham surgery at each time point. Top 2 and bottom 2 panels represent sequential imaging data of TAC and sham-surgery mice, respectively. Sequential imaging of the 6 other surgically treated mice is shown in Supplemental Fig. S3. Insets in images show magnified images of the heart. Color scale depends on the ratio relative to brain intensity. *E*) Cardiac-specific enhancer activity plots of 10 Tg-line1 mice (TAC1, TAC2, and Sham1, Sham2, shown in *D*) and TAC3–5 and Sham3–5 shown in Supplemental Fig. S3). Heart to brain luciferase intensity ratio represents the cardiac-specific enhancer activity; enhancer activity in presurgery mice was defined as 1. 3 wk after TAC surgery: 5.7 ± 1.3 fold; 3 wk after sham surgery: 1.0 ± 0.2 fold; means ± SE; n = 5. *$P < 0.001$, repeated ANOVA.

mice enabled us to accurately quantify the expression level of the natriuretic peptides. These mice are useful tools for repeatedly assessing the degree of heart failure to screen various cardiovascular drugs.

The integration of activities from multiple enhancers could confer specificity and robustness to transcriptional regulation (1). Warren *et al.* (14) identified the *Nppa* enhancer in the embryonic heart by examining Nkx2-5 binding regions around the *Nppa* locus, but the enhancer did not respond to heart failure. This enhancer does not overlap with CR9 and might regulate *Nppa* expression only during the embryonic stage (14). On the other hand, Horsthuis *et al.* (11) showed that the regulatory region from −27 to +58 kb relative to the transcription start site of *Nppa* was sufficient for *Nppa* gene expression in the failing heart, similar to CR9. However, because this 85-kb regulatory region does not include CR9, *Nppa* may have multiple enhanc-

ers that regulate its expression during heart failure. Furthermore, the length of the 85-kb region poses a challenge for understanding its specific biological role.

This is the first study to provide a time course imaging analysis of enhancer activity using an individual live diseased mouse model. Using this new method, we identified a novel heart enhancer. This method can be widely used for identifying enhancers that regulate transcriptional activity only under pathological conditions. FJ

This research was supported by the Japan Society for the Promotion of Science (JSPS) through the Funding Program for Next Generation World-Leading Researchers (NEXT Program), which was initiated by the Council for Science and Technology Policy (CSTP); grants-in-aid from the Ministry of Health, Labor, and Welfare of Japan; grants-in-aid from the Ministry of Education, Culture, Sports, Science, and Technology of Japan; and grants-in-aid from the Japan Society for the Promotion of Science. This research was also supported by grants from the Japan Heart Foundation, the Japan Cardiovascular Research Foundation, the Japan Medical Association, the Japan Intractable Diseases Research Foundation, the Uehara Memorial Foundation, the Takeda Science Foundation, the Ichiro Kanehara Foundation, the Inoue Foundation for Science, the Mochida Memorial Foundation, a Heart Foundation/Novartis Grant for Research Award on Molecular and Cellular Cardiology, the Japan Foundation of Applied Enzymology, the Naito Foundation, the Banyu Foundation, and Showa Houkoukai. The authors thank Hiroshi Kimura for antibodies, Seitaro Nomura for the ChIP-seq analysis, Saori Ikezawa and Eri Takata for technical assistance, and Yuko Okada and Hiromi Fujii for secretarial support.

REFERENCES

1. Spitz, F., and Furlong, E. E. (2012) Transcription factors: from enhancer binding to developmental control. *Nat. Rev. Genet.* **13,** 613–626
2. Chien, K. R., Domian, I. J., and Parker, K. K. (2008) Cardiogenesis and the complex biology of regenerative cardiovascular medicine. *Science* **322,** 1494–1497
3. Olson, E. N. (2006) Gene regulatory networks in the evolution and development of the heart. *Science* **313,** 1922–1927
4. Burley, D. S., and Baxter, G. F. (2007) B-type natriuretic peptide at early reperfusion limits infarct size in the rat isolated heart. *Basic Res. Cardiol.* **102,** 529–541
5. Holtwick, R., van Eickels, M., Skryabin, B. V., Baba, H. A., Bubikat, A., Begrow, F., Schneider, M. D., Garbers, D. L., and Kuhn, M. (2003) Pressure-independent cardiac hypertrophy in mice with cardiomyocyte-restricted inactivation of the atrial natriuretic peptide receptor guanylyl cyclase-A. *J. Clin. Invest.* **111,** 1399–1407
6. Kitakaze, M., Asakura, M., Kim, J., Shintani, Y., Asanuma, H., Hamasaki, T., Seguchi, O., Myoishi, M., Minamino, T., Ohara, T., Nagai, Y., Nanto, S., Watanabe, K., Fukuzawa, S., Hirayama, A., Nakamura, N., Kimura, K., Fujii, K., Ishihara, M., Saito, Y., Tomoike, H., and Kitamura, S. (2007) Human atrial natriuretic peptide and nicorandil as adjuncts to reperfusion treatment for acute myocardial infarction (J-WIND): two randomised trials. *Lancet* **370,** 1483–1493
7. Li, P., Wang, D., Lucas, J., Oparil, S., Xing, D., Cao, X., Novak, L., Renfrow, M. B., and Chen, Y. F. (2008) Atrial natriuretic peptide inhibits transforming growth factor beta-induced Smad signaling and myofibroblast transformation in mouse cardiac fibroblasts. *Circ. Res.* **102,** 185–192
8. Tamura, N., Ogawa, Y., Chusho, H., Nakamura, K., Nakao, K., Suda, M., Kasahara, M., Hashimoto, R., Katsuura, G., Mukoyama, M., Itoh, H., Saito, Y., Tanaka, I., Otani, H., and Katsuki, M. (2000) Cardiac fibrosis in mice lacking brain natriuretic peptide. *Proc. Natl. Acad. Sci. U. S. A.* **97,** 4239–4244
9. De Lange, F. J., Moorman, A. F., and Christoffels, V. M. (2003) Atrial cardiomyocyte-specific expression of Cre recombinase driven by an Nppa gene fragment. *Genesis* **37,** 1–4
10. Habets, P. E., Moorman, A. F., Clout, D. E., van Roon, M. A., Lingbeek, M., van Lohuizen, M., Campione, M., and Christoffels, V. M. (2002) Cooperative action of Tbx2 and Nkx2.5 inhibits ANF expression in the atrioventricular canal: implications for cardiac chamber formation. *Genes Dev.* **16,** 1234–1246
11. Horsthuis, T., Houweling, A. C., Habets, P. E., de Lange, F. J., el Azzouzi, H., Clout, D. E., Moorman, A. F., and Christoffels, V. M. (2008) Distinct regulation of developmental and heart disease-induced atrial natriuretic factor expression by two separate distal sequences. *Circ. Res.* **102,** 849–859
12. Knowlton, K. U., Rockman, H. A., Itani, M., Vovan, A., Seidman, C. E., and Chien, K. R. (1995) Divergent pathways mediate the induction of ANF transgenes in neonatal and hypertrophic ventricular myocardium. *J. Clin. Invest.* **96,** 1311–1318
13. Small, E. M., and Krieg, P. A. (2003) Transgenic analysis of the atrialnatriuretic factor (ANF) promoter: Nkx2-5 and GATA-4 binding sites are required for atrial specific expression of ANF. *Dev. Biol.* **261,** 116–131
14. Warren, S. A., Terada, R., Briggs, L. E., Cole-Jeffrey, C. T., Chien, W. M., Seki, T., Weinberg, E. O., Yang, T. P., Chin, M. T., Bungert, J., and Kasahara, H. (2011) Differential role of Nkx2-5 in activation of the atrial natriuretic factor gene in the developing versus failing heart. *Mol. Cell. Biol.* **31,** 4633–4645
15. Simpson, P., McGrath, A., and Savion, S. (1982) Myocyte hypertrophy in neonatal rat heart cultures and its regulation by serum and by catecholamines. *Circ. Res.* **51,** 787–801
16. Siepel, A., Bejerano, G., Pedersen, J. S., Hinrichs, A. S., Hou, M., Rosenbloom, K., Clawson, H., Spieth, J., Hillier, L. W., Richards, S., Weinstock, G. M., Wilson, R. K., Gibbs, R. A., Kent, W. J., Miller, W., and Haussler, D. (2005) Evolutionarily conserved elements in vertebrate, insect, worm, and yeast genomes. *Genome Res.* **15,** 1034–1050
17. Blanchette, M., Kent, W. J., Riemer, C., Elnitski, L., Smit, A. F., Roskin, K. M., Baertsch, R., Rosenbloom, K., Clawson, H., Green, E. D., Haussler, D., and Miller, W. (2004) Aligning multiple genomic sequences with the threaded blockset aligner. *Genome Res.* **14,** 708–715
18. Pollard, K. S., Hubisz, M. J., Rosenbloom, K. R., and Siepel, A. (2010) Detection of nonneutral substitution rates on mammalian phylogenies. *Genome Res.* **20,** 110–121
19. Zhang, Y., Liu, T., Meyer, C. A., Eeckhoute, J., Johnson, D. S., Bernstein, B. E., Nusbaum, C., Myers, R. M., Brown, M., Li, W., and Liu, X. S. (2008) Model-based analysis of ChIP-Seq (MACS). *Genome Biol.* **9,** R137
20. Dekker, J., Rippe, K., Dekker, M., and Kleckner, N. (2002) Capturing chromosome conformation. *Science* **295,** 1306–1311
21. Hagege, H., Klous, P., Braem, C., Splinter, E., Dekker, J., Cathala, G., de Laat, W., and Forne, T. (2007) Quantitative analysis of chromosome conformation capture assays (3C-qPCR). *Nat. Protoc.* **2,** 1722–1733
22. Liao, Y., Ishikura, F., Beppu, S., Asakura, M., Takashima, S., Asanuma, H., Sanada, S., Kim, J., Ogita, H., Kuzuya, T., Node, K., Kitakaze, M., and Hori, M. (2002) Echocardiographic assessment of LV hypertrophy and function in aortic-banded mice: necropsy validation. *Am. J. Physiol. Heart Circ. Physiol.* **282,** H1703–H1708
23. Saadane, N., Alpert, L., and Chalifour, L. E. (1999) Expression of immediate early genes, GATA-4, and Nkx-2.5 in adrenergic-induced cardiac hypertrophy and during regression in adult mice. *Brit. J. Pharmacol.* **127,** 1165–1176
24. Vecchione, C., Fratta, L., Rizzoni, D., Notte, A., Poulet, R., Porteri, E., Frati, G., Guelfi, D., Trimarco, V., Mulvany, M. J., Agabiti-Rosei, E., Trimarco, B., Cotecchia, S., and Lembo, G. (2002) Cardiovascular influences of $\alpha 1\beta$-adrenergic receptor defect in mice. *Circulation* **105,** 1700–1707
25. Nobrega, M. A., Ovcharenko, I., Afzal, V., and Rubin, E. M. (2003) Scanning human gene deserts for long-range enhancers. *Science* **302,** 413
26. Thomas, J. W., Touchman, J. W., Blakesley, R. W., Bouffard, G. G., Beckstrom-Sternberg, S. M., Margulies, E. H., Blanchette, M., Siepel, A. C., Thomas, P. J., McDowell, J. C., Maskeri, B., Hansen, N. F., Schwartz, M. S., Weber, R. J., Kent, W. J.,

Karolchik, D., Bruen, T. C., Bevan, R., Cutler, D. J., Schwartz, S., Elnitski, L., Idol, J. R., Prasad, A. B., Lee-Lin, S. Q., Maduro, V. V., Summers, T. J., Portnoy, M. E., Dietrich, N. L., Akhter, N., Ayele, K., Benjamin, B., Cariaga, K., Brinkley, C. P., Brooks, S. Y., Granite, S., Guan, X., Gupta, J., Haghighi, P., Ho, S. L., Huang, M. C., Karlins, E., Laric, P. L., Legaspi, R., Lim, M. J., Maduro, Q. L., Masiello, C. A., Mastrian, S. D., McCloskey, J. C., Pearson, R., Stantripop, S., Tiongson, E. E., Tran, J. T., Tsurgeon, C., Vogt, J. L., Walker, M. A., Wetherby, K. D., Wiggins, L. S., Young, A. C., Zhang, L. H., Osoegawa, K., Zhu, B., Zhao, B., Shu, C. L., De Jong, P. J., Lawrence, C. E., Smit, A. F., Chakravarti, A., Haussler, D., Green, P., Miller, W., and Green, E. D. (2003) Comparative analyses of multi-species sequences from targeted genomic regions. *Nature* **424,** 788–793

27. Woolfe, A., Goodson, M., Goode, D. K., Snell, P., McEwen, G. K., Vavouri, T., Smith, S. F., North, P., Callaway, H., Kelly, K., Walter, K., Abnizova, I., Gilks, W., Edwards, Y. J., Cooke, J. E., and Elgar, G. (2005) Highly conserved non-coding sequences are associated with vertebrate development. *PLoS Biol.* **3,** e7
28. Bell, A. C., West, A. G., and Felsenfeld, G. (1999) The protein CTCF is required for the enhancer blocking activity of vertebrate insulators. *Cell* **98,** 387–396
29. Felsenfeld, G., Burgess-Beusse, B., Farrell, C., Gaszner, M., Ghirlando, R., Huang, S., Jin, C., Litt, M., Magdinier, F., Mutskov, V., Nakatani, Y., Tagami, H., West, A., and Yusufzai, T. (2004) Chromatin boundaries and chromatin domains. *Cold Spring Harb. Symp. Quant. Biol.* **69,** 245–250
30. Shen, Y., Yue, F., McCleary, D. F., Ye, Z., Edsall, L., Kuan, S., Wagner, U., Dixon, J., Lee, L., Lobanenkov, V. V., and Ren, B. (2012) A map of the cis-regulatory sequences in the mouse genome. *Nature* **488,** 116–120
31. Birney, E., Stamatoyannopoulos, J. A., Dutta, A., Guigo, R., Gingeras, T. R., Margulies, E. H., Weng, Z., Snyder, M., Dermitzakis, E. T., Thurman, R. E., Kuehn, M. S., Taylor, C. M., Neph, S., Koch, C. M., Asthana, S., Malhotra, A., Adzhubei, I., Greenbaum, J. A., Andrews, R. M., Flicek, P., Boyle, P. J., Cao, H., Carter, N. P., Clelland, G. K., Davis, S., Day, N., Dhami, P., Dillon, S. C., Dorschner, M. O., Fiegler, H., Giresi, P. G., Goldy, J., Hawrylycz, M., Haydock, A., Humbert, R., James, K. D., Johnson, B. E., Johnson, E. M., Frum, T. T., Rosenzweig, E. R., Karnani, N., Lee, K., Lefebvre, G. C., Navas, P. A., Neri, F., Parker, S. C., Sabo, P. J., Sandstrom, R., Shafer, A., Vetrie, D., Weaver, M., Wilcox, S., Yu, M., Collins, F. S., Dekker, J., Lieb, J. D., Tullius, T. D., Crawford, G. E., Sunyaev, S., Noble, W. S., Dunham, I., Denoeud, F., Reymond, A., Kapranov, P., Rozowsky, J., Zheng, D., Castelo, R., Frankish, A., Harrow, J., Ghosh, S., Sandelin, A., Hofacker, I. L., Baertsch, R., Keefe, D., Dike, S., Cheng, J., Hirsch, H. A., Sekinger, E. A., Lagarde, J., Abril, J. F., Shahab, A., Flamm, C., Fried, C., Hackermuller, J., Hertel, J., Lindemeyer, M., Missal, K., Tanzer, A., Washietl, S., Korbel, J., Emanuelsson, O., Pedersen, J. S., Holroyd, N., Taylor, R., Swarbreck, D., Matthews, N., Dickson, M. C., Thomas, D. J., Weirauch, M. T., Gilbert, J., Drenkow, J., Bell, I., Zhao, X., Srinivasan, K. G., Sung, W. K., Ooi, H. S., Chiu, K. P., Foissac, S., Alioto, T., Brent, M., Pachter, L., Tress, M. L., Valencia, A., Choo, S. W., Choo, C. Y., Ucla, C., Manzano, C., Wyss, C., Cheung, E., Clark, T. G., Brown, J. B., Ganesh, M., Patel, S., Tammana, H., Chrast, J., Henrichsen, C. N., Kai, C., Kawai, J., Nagalakshmi, U., Wu, J., Lian, Z., Lian, J., Newburger, P., Zhang, X., Bickel, P., Mattick, J. S., Carninci, P., Hayashizaki, Y., Weissman, S., Hubbard, T., Myers, R. M., Rogers, J., Stadler, P. F., Lowe, T. M., Wei, C. L., Ruan, Y., Struhl, K., Gerstein, M., Antonarakis, S. E., Fu, Y., Green, E. D., Karaoz, U., Siepel, A., Taylor, J., Liefer, L. A., Wetterstrand, K. A., Good, P. J., Feingold, E. A., Guyer, M. S., Cooper, G. M., Asimenos, G., Dewey, C. N., Hou, M., Nikolaev, S., Montoya-Burgos, J. I., Loytynoja, A., Whelan, S., Pardi, F., Massingham, T., Huang, H., Zhang, N. R., Holmes, I., Mullikin, J. C., Ureta-Vidal, A., Paten, B., Seringhaus, M., Church, D., Rosenbloom, K., Kent, W. J., Stone, E. A., Batzoglou, S., Goldman, N., Hardison, R. C., Haussler, D., Miller, W., Sidow, A., Trinklein, N. D., Zhang, Z. D., Barrera, L., Stuart, R., King, D. C., Ameur, A., Enroth, S., Bieda, M. C., Kim, J., Bhinge, A. A., Jiang, N., Liu, J., Yao, F., Vega, V. B., Lee, C. W., Ng, P., Shahab, A., Yang, A., Moqtaderi, Z., Zhu, Z., Xu, X., Squazzo, S., Oberley, M. J., Inman, D., Singer, M. A., Richmond, T. A., Munn, K. J., Rada-Iglesias, A., Wallerman, O., Komorowski, J., Fowler, J. C., Couttet, P., Bruce, A. W., Dovey, O. M., Ellis, P. D., Langford, C. F., Nix, D. A., Euskirchen, G., Hartman, S., Urban, A. E., Kraus, P., Van Calcar, S., Heintzman, N., Kim, T. H., Wang, K., Qu, C., Hon, G., Luna, R., Glass, C. K., Rosenfeld, M. G., Aldred, S. F., Cooper, S. J., Halees, A., Lin, J. M., Shulha, H. P., Zhang, X., Xu, M., Haidar, J. N., Yu, Y., Ruan, Y., Iyer, V. R., Green, R. D., Wadelius, C., Farnham, P. J., Ren, B., Harte, R. A., Hinrichs, A. S., Trumbower, H., Clawson, H., Hillman-Jackson, J., Zweig, A. S., Smith, K., Thakkapallayil, A., Barber, G., Kuhn, R. M., Karolchik, D., Armengol, L., Bird, C. P., de Bakker, P. I., Kern, A. D., Lopez-Bigas, N., Martin, J. D., Stranger, B. E., Woodroffe, A., Davydov, E., Dimas, A., Eyras, E., Hallgrimsdottir, I. B., Huppert, J., Zody, M. C., Abecasis, G. R., Estivill, X., Bouffard, G. G., Guan, X., Hansen, N. F., Idol, J. R., Maduro, V. V., Maskeri, B., McDowell, J. C., Park, M., Thomas, P. J., Young, A. C., Blakesley, R. W., Muzny, D. M., Sodergren, E., Wheeler, D. A., Worley, K. C., Jiang, H., Weinstock, G. M., Gibbs, R. A., Graves, T., Fulton, R., Mardis, E. R., Wilson, R. K., Clamp, M., Cuff, J., Gnerre, S., Jaffe, D. B., Chang, J. L., Lindblad-Toh, K., Lander, E. S., Koriabine, M., Nefedov, M., Osoegawa, K., Yoshinaga, Y., Zhu, B., and de Jong, P. J. (2007) Identification and analysis of functional elements in 1% of the human genome by the ENCODE pilot project. *Nature* **447,** 799–816
32. Blow, M. J., McCulley, D. J., Li, Z., Zhang, T., Akiyama, J. A., Holt, A., Plajzer-Frick, I., Shoukry, M., Wright, C., Chen, F., Afzal, V., Bristow, J., Ren, B., Black, B. L., Rubin, E. M., Visel, A., and Pennacchio, L. A. (2010) ChIP-Seq identification of weakly conserved heart enhancers. *Nat. Genet.* **42,** 806–810
33. Koch, F., Jourquin, F., Ferrier, P., and Andrau, J. C. (2008) Genome-wide RNA polymerase II: not genes only!. *Trends Biochem. Sci.* **33,** 265–273
34. Szutorisz, H., Dillon, N., and Tora, L. (2005) The role of enhancers as centres for general transcription factor recruitment. *Trends Biochem. Sci.* **30,** 593–599
35. Sei, C. A., Irons, C. E., Sprenkle, A. B., McDonough, P. M., Brown, J. H., and Glembotski, C. C. (1991) The α-adrenergic stimulation of atrial natriuretic factor expression in cardiac myocytes requires calcium influx, protein kinase C, and calmodulin-regulated pathways. *J. Biol. Chem.* **266,** 15910–15916
36. Iaccarino, G., Dolber, P. C., Lefkowitz, R. J., and Koch, W. J. (1999) Bβ-adrenergic receptor kinase-1 levels in catecholamine-induced myocardial hypertrophy: regulation by beta- but not alpha1-adrenergic stimulation. *Hypertension* **33,** 396–401
37. Seidman, C. E., Wong, D. W., Jarcho, J. A., Bloch, K. D., and Seidman, J. G. (1988) *Cis*-acting sequences that modulate atrial natriuretic factor gene expression. *Proc. Natl. Acad. Sci. U. S. A.* **85,** 4104–4108
38. Thuerauf, D. J., and Glembotski, C. C. (1997) Differential effects of protein kinase C, Ras, and Raf-1 kinase on the induction of the cardiac B-type natriuretic peptide gene through a critical promoter-proximal M-CAT element. *J. Biol. Chem.* **272,** 7464–7472

Received for publication November 12, 2013.
Accepted for publication January 2, 2014.

Matsuoka_Supplemental Figure S1

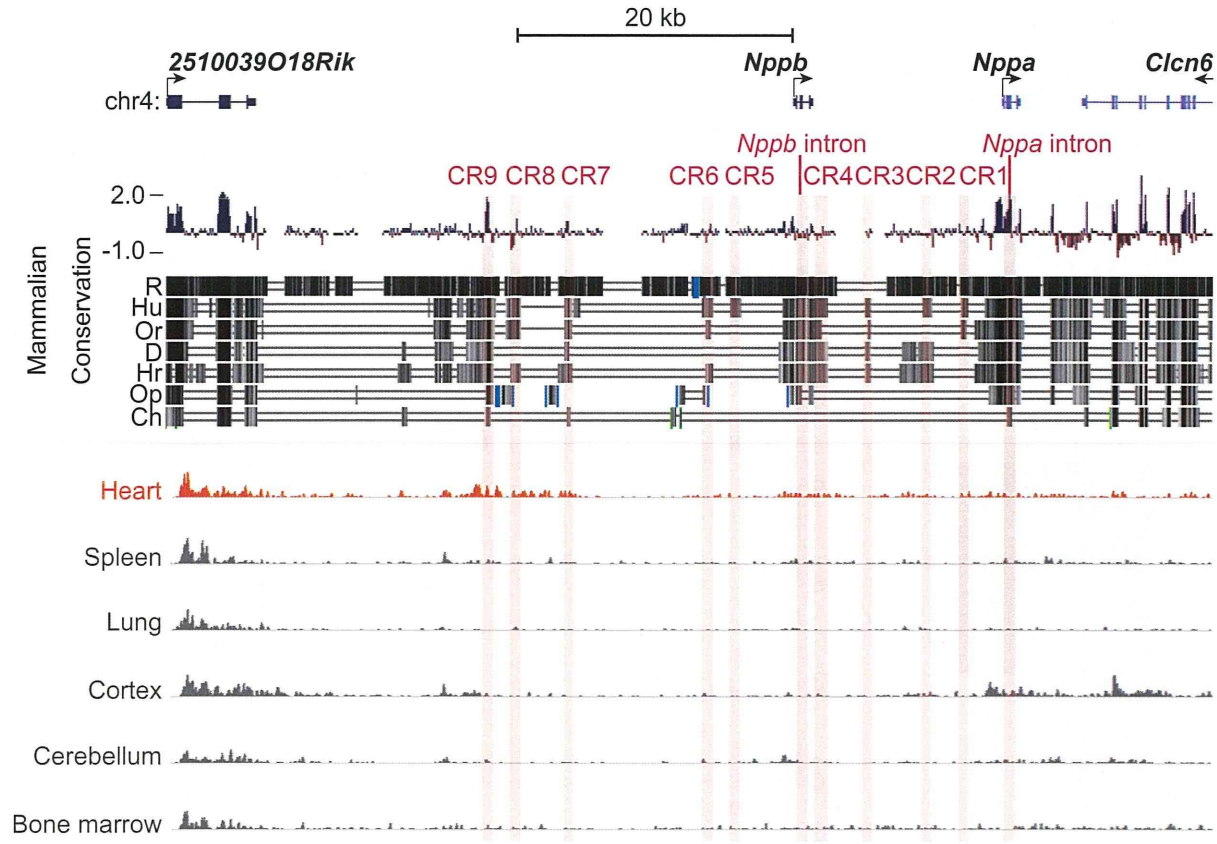

Supplemental Figure S1. CR9 overlapped with the gene region that is modified by H3K4me1 in a cardiac-specific manner. Mammalian evolutionarily conserved regions (CRs) and ChIP-seq data for H3K4me1 surrounding the murine *Nppa* and *Nppb* loci. Non-coding conserved regions are highlighted as light red vertical bars (CR1-9, *Nppa* intron, and *Nppb* intron). ChIP-seq data for H3K4me1 in various organs was obtained from an open database of the adult mouse heart. R, Rat; Hu, Human; Or, Orangutan; D, Dog; Hr, Horse; Op, Opossum; Ch, Chicken.

Matsuoka_Supplemental Figure S2

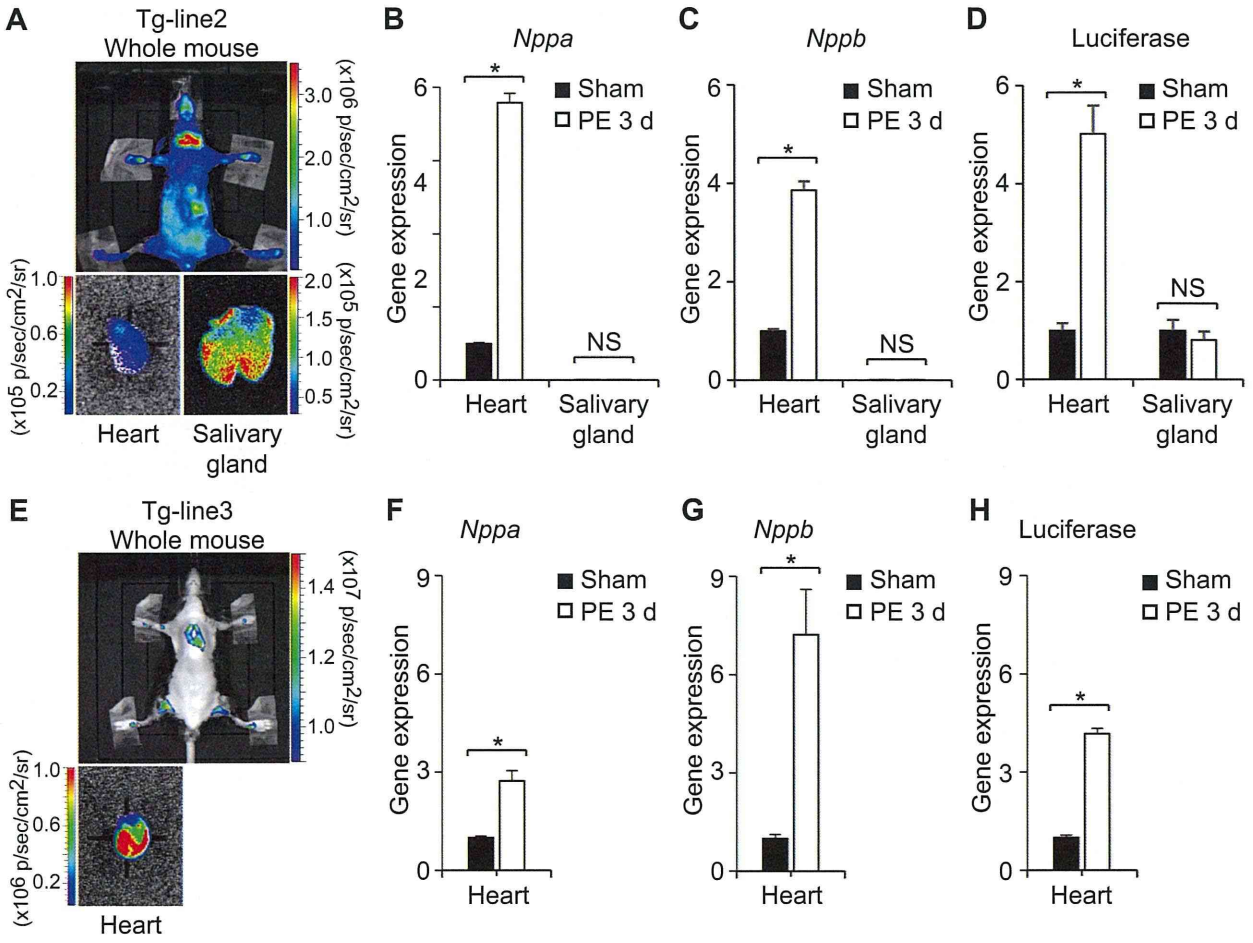

Supplemental Figure S2. The luciferase reporter expressions in mice of Tg-line2 and Tg-line3. (***A***) Chemiluminescence imaging of CR9 in a mouse of Tg-line2. The upper panel shows the result from whole animal *in vivo* live imaging. The lower left and right panels show the chemiluminescence images of the heart and salivary glands in the same mouse. (***B***) (***C***) The relative transcript levels of *Nppa* and *Nppb* in the ventricular myocardium and salivary glands of CR9 Tg-line2 mice treated with continuous infusion of phenylephrine (PE) for 3 days. The average transcript level in the ventricular myocardium of pre-infused mice was defined as 1. (means ± SEM, n = 3) * represents a significant difference relative to sham-infused mice at $P < 0.01$, *t*-test. (***D***) The relative transcript levels of the luciferase reporter in the ventricular myocardium and salivary glands of the CR9 Tg-line2 mice continuously infused with PE for 3 days. The average transcript level in the ventricular myocardium and brain of pre-infused mice was defined as 1. (means ± SEM, n = 3) * represents a significant difference relative to the sham mice at $P < 0.01$, *t*-test. (***E***) Chemiluminescence imaging of CR9 in a mouse of Tg-line3. The upper panel shows the result from whole animal *in vivo* live imaging. The lower panel shows the chemiluminescence image of the heart in the same mouse. (***F***) (***G***) (***H***) The relative transcript levels of *Nppa*, *Nppb*, and luciferase reporter in the ventricular myocardium of CR9 Tg-line3 mice treated with continuous infusion of PE for 3 days. The average transcript level in the ventricular myocardium of pre-infused mice was defined as 1. (means ± SEM, n = 3) * represents a significant difference relative to sham-infused mice at $P < 0.01$, *t*-test.

Matsuoka_Supplemental Figure S3

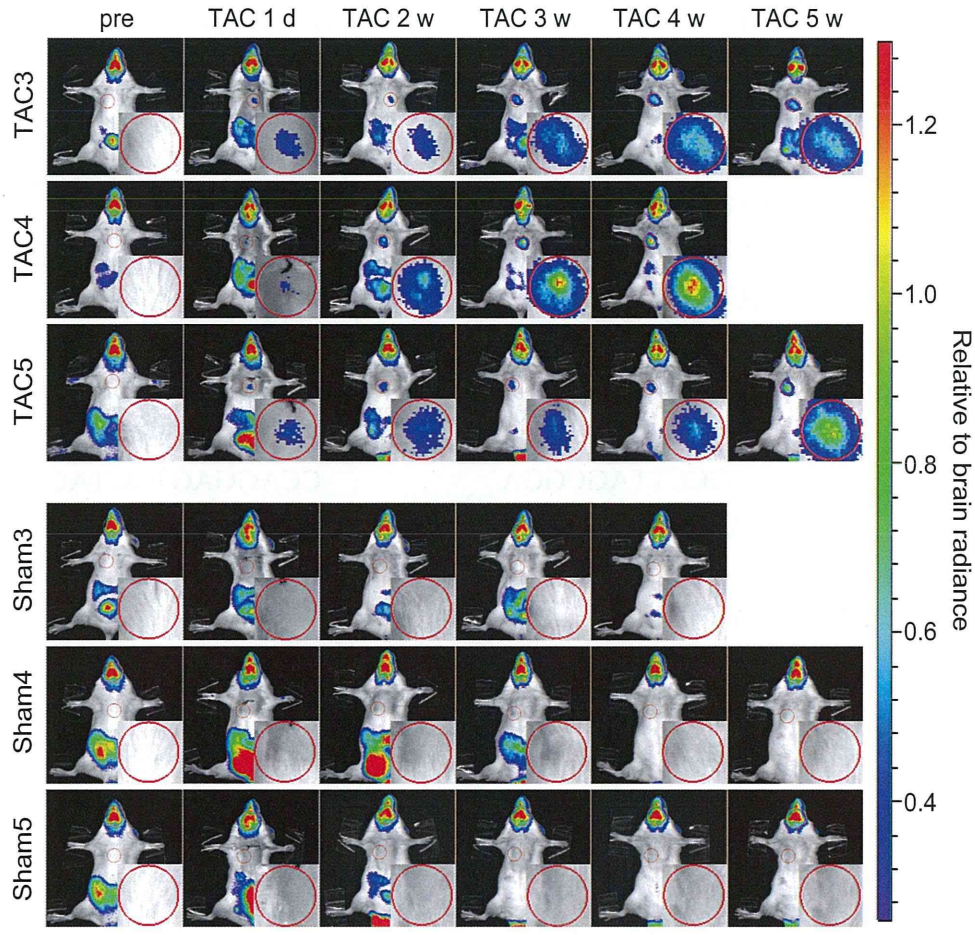

Supplemental Figure S3. Sequential *in vivo* live imaging of six Tg-line1 mice before and after TAC or sham operation at each time point. The upper three panels and lower three panels represent the sequential imaging data of TAC and sham mice, respectively. The outlined images in the lower right are magnified images of the heart. The color scale depends on the ratio relative to brain luciferase intensity.

Supplemental Table S1. Oligonucleotide primers for the enhancer reporter assays.

Target	Location*	Forward primer	Reverse primer
CR1	-2961 / -1146	GATCGATGCCTTAAACTC CTGA	GTGGAGTTGTCATGTGG CTGGA
CR2	-5926 / -4141	GATCGATAGAAGCCAGGA CAGT	GGTGGTGTAGTGGGTAA ATGCC
CR3	-9897 / -9275	AGTTCAAGGCCAGTGTGA GGTGATGACTCT	GAATAGGAACAGGGAGC CACTGTCCAGTGA
CR4	-13843 / -12368	CGGCACCTGCTTCAGTTTC ACTTCCGAGTGT	TGGGTGTGAGACCCATG CAAGGCAAGTGCT
CR5	-19743 /-18381	CAGAGAATGCTACCTGAA GACAGAGGTGAGA	GCGCTTAACATATGGGA ACACATTCCAACA
CR6	-22306 / -20539	CAAGGACACCAGTCTGAC TGGCCTTAGCGGA	TCCCCAGTGAACAAATC CCAGGAGTGGTAGCA
CR7	-31531 / -30882	GAATTCGGGTATGCTGCC CTAAGCTGCT	ACTAGTGTAGCTTTGTGA GACTGTGAGCA
CR8	-35258 / -34526	CACTAGTTACACTCTTGG GTGCAGGGATCA	TTCAGGTCCTGTGGGGC ATTGCTAAGTGGA
CR9	-37185 / -36536	TACTAGTCTCATGGTGCC AGTTGCTGCCCT	ATCCTAGGCCCTTCCTGG TTTATCTCCCAG
Nppa intron	189 / 1052	CAGATCTGATGGATTTCA AGGTAGGGCCA	CCTCCTTGGCTGTTATCT TCGGTACTACA
Nppb intron	-14664 / -13760	CAGAGCAATTCAAGATGC AGGTGAGCACT	AGGTCTTCCTACAACAA CTTCAGTGCTGT
Nppb promoter	-14968 / -14771	CCTGAGCTCAGCCGGCAG GAATGCAGCTGAT	TGGATCCGCCGCAGAAG CGATGGGCCA

*Location from the *Nppa* transcription start site.

Supplemental Table S2. Oligonucleotide primers and probes for the 3C assay.

Primer or probe name	Location*	Sequence
1 forward	-29092	GTGTGAGCAGAGGCCAAGGTATA
2 forward	-36590	CCATCTTGGAACCTGGTGGTT
3 forward	-38677	GAGGTGCTATCTGCCACTGGTT
4 forward	-42755	GCAGAAAAGAGGGTAATTTAGCTCCT
Nppa promoter reverse	-4376	GTTCAATTCCCAGCAACCACAT
Nppb promoter reverse	-20204	CTTATATATGCAATGGTGTCAGCACTT
Probe for *Nppa*	-4420	ATAACAGATGATTGTGAGCCAC
Probe for *Nppb*	-20248	ATCCCATAATCAGCCCC

*Location from the *Nppa* transcription start site.

International Journal of Cardiology 172 (2014) e288–e289

Contents lists available at ScienceDirect

International Journal of Cardiology

journal homepage: www.elsevier.com/locate/ijcard

Letter to the Editor

Comprehensive metagenomic approach for detecting causative microorganisms in culture-negative infective endocarditis

Atsuko Imai [a], Kazuyoshi Gotoh [b], Yoshihiro Asano [a,*], Noriaki Yamada [a], Daisuke Motooka [b], Masaki Fukushima [a], Machiko Kanzaki [a], Tomohito Ohtani [a], Yasushi Sakata [a], Hiroyuki Nishi [c], Koichi Toda [c], Yoshiki Sawa [c], Issei Komuro [a], Toshihiro Horii [b], Tetsuya Iida [b], Shota Nakamura [b], Seiji Takashima [a,d]

[a] Department of Cardiovascular Medicine, Osaka University Graduate School of Medicine, Suita, Osaka, Japan
[b] Department of Infection Metagenomics, Research Institute for Microbial Diseases, Osaka University, Suita, Osaka, Japan.
[c] Department of Cardiovascular Surgery, Osaka University Graduate School of Medicine, Suita, Osaka, Japan
[d] Department of Medical Biochemistry, Osaka University Graduate School of Medicine, Suita, Osaka, Japan

ARTICLE INFO

Article history:
Received 14 November 2013
Accepted 28 December 2013
Available online 8 January 2014

Keywords:
Metagenomic analysis
Culture-negative infective endocarditis
Next generation sequencing

A recent nationwide survey of infective endocarditis (IE) showed that IE is still a lethal disease, with an in-hospital death rate of 11% [1]. Detecting causative microorganisms plays an important role in choosing optimal antibiotics and effective dosing periods [2]. However, culture-negative IE was frequently observed, especially among cases that included premedication with antimicrobial agents [3]. Previous studies reported that valve culture has low sensitivity between 8% and 13% [4,5]. Furthermore, valve culture can detect only viable and target microorganisms with the culture medium currently available. Recently, the metagenomic approach using Next Generation Sequencing (NGS) emerged as a comprehensive method for exploring causative agents of infectious diseases without prior culture [6]. Therefore, we assessed the viability of metagenomic approach to detect causative microorganisms in resected valves from IE patients.

We conducted metagenomic analyses using NGS technology for resected valves in 3 IE cases. Between May 2012 and February 2013, 3 IE patients who had been admitted to the cardiovascular department at Osaka University, Suita, Japan, underwent metagenomic analyses of resected valves. Case 1 is a 55-year-old female with IE of the native aortic valve. Case 2 is a 57-year-old male who presented with IE of both native aortic and mitral valves. Case 3 is a 74-year-old female with IE of the native aortic valve.

We extracted DNA from the homogenized valve using the QIAamp cador Pathogen Mini kit (QIAGEN). Using the Nextera DNA sample preparation kit (Illumina), a sequencing library was prepared from the extracted DNA. We then performed metagenomic shotgun sequencing on the MiSeq platform (Illumina) according to the manufacturer's protocol. Obtained reads were trimmed of low-quality sequences and subjected to the NCBI BLAST search against the Genbank nt database. We assigned taxonomy based on the NCBI taxonomy database.

In 2 culture-positive cases, metagenomic results of resected valves were consistent with cultivation results. In case 1, the blood culture at the primary hospital was positive for *Enterococcus faecalis* after administration of several antibiotics and negative at the time of referral to our hospital. The resected valve culture was also positive for *E. faecalis*. In case 2, both the blood and valve cultures were positive for *Streptococcus mutans* without any prior administration of antibiotics. The results of metagenomic sequencing of resected aortic valves were summarized in Table 1. In both cases, the dominant parts in bacteria-derived sequences could be mapped on the genomes of candidate bacterial species using BLAST search, *E. faecalis* and *S. mutans* respectively

Table 1
Summary of the sequencing results of resected aortic valves.

	Case 1		Case 2*		Case 3	
	no.	(%)	no.	(%)	no.	(%)
Total reads	327,913	100.0	322,497	100.0	425,706	100.0
Reads from human genome	314,507	95.9	319,257	99.0	410,300	96.4
Reads from bacterial genome						
	E. faecalis (NC_019770)		S. mutans (NC_013928)		S. sanguinis (NC_009009)	
	2251	0.68	145	0.047	72	0.017

* Metagenomic analysis of resected mitral valve also detected *Streptococcus mutans*.

* Corresponding author at: Department of Cardiovascular Medicine, Osaka University Graduate School of Medicine, 2-2 Yamadaoka, Suita, Osaka 565-0871, Japan. Tel.: +81 6 6879 3492; fax: +81 6 6879 3493.
E-mail address: asano@cardiology.med.osaka-u.ac.jp (Y. Asano).

http://dx.doi.org/10.1016/j.ijcard.2013.12.197

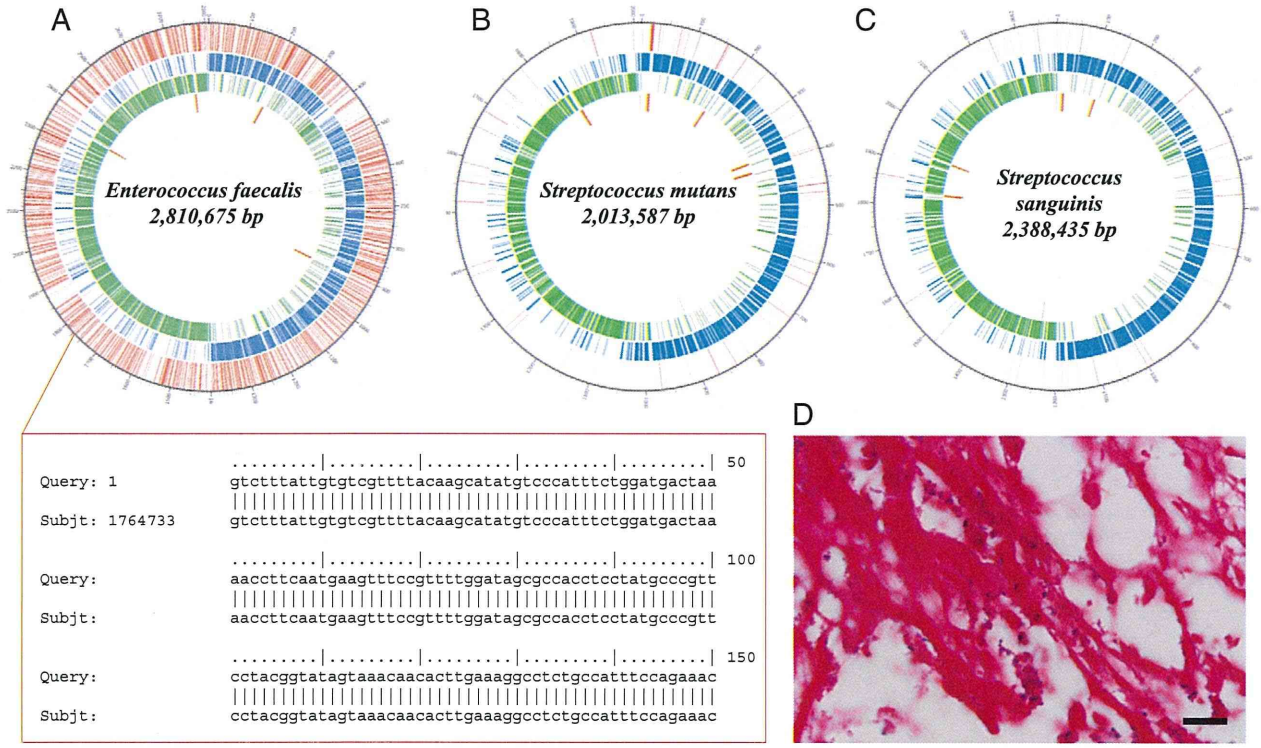

Fig. 1. (A–C) Circular genome maps of target bacteria. Outer layer shows fragments detected in each analysis (Red), the second outer layer, positive strand genes of target bacteria (Blue); the third outer layer, negative strand genes of target bacteria (Green); the fourth outer layer, ribosomal/transfer RNA of target bacteria (Orange). Reference genome maps of *Enterococcus faecalis* for case 1 (A), *Streptococcus mutans* for case 2 (B), and *Streptococcus sanguinis* for case 3 (C), respectively. Representative sequences detected by NGS technology was shown in A. (D) Gram-staining of the resected valve tissue in case 3 Gram-positive cocci were identified indicated. Scale bar;10 μM.

(Fig. 1A, B). Metagenomic results were consistent with culture results in both cases.

Besides culture positive cases, the metagenomic approach could also detect causative organism of IE in 1 culture-negative case. In case 3, both the blood and valve cultures were negative at our hospital after the patient took several antibiotics prior to admission. Genome mapping using metagenomic data showed *Streptococcus sanguinis* as a causative bacterium (Fig. 1C). It was confirmed by Gram-staining, in which Gram-positive cocci were identified in the valve tissue (Fig. 1D).

To our knowledge, this is the first report to successfully identify bacterial genome fragments using NGS and to show the superiority of this approach over valve culture in detecting microorganisms in culture-negative IE.

In general, there are three major advantages of NGS metagenomic analysis in detecting causative microorganisms of IE compared to conventional methods. First, metagenomic shotgun sequencing by NGS can screen for various microorganisms, including viruses and fungi, whereas targeted amplicon sequencing such as 16S rRNA sequencing can only screen for bacteria [7]. Second, metagenomic NGS analysis can detect nonviable or unculturable microorganisms as long as microbial nucleic acids remain in the specimen, which overcomes the limitation of low sensitivity in conventional culture-based methods. Thirdly, unlike the 16S rRNA analysis, it can yield high-throughput sequence reads covering genome-wide regions, which has a potential to be used for multi-locus sequence typing analysis [8]. All these advantages indicate promising clinical application of this method.

Although studies with larger samples are required to confirm the validity of our initial results, our results showed the possibility metagenomic shotgun sequencing by NGS can be added to current screening methods for detecting microorganisms, especially in culture-negative IE.

The authors of this manuscript have certified that they comply with the Principles of Ethical Publishing in the International Journal of Cardiology.

References

[1] Nakatani S, Mitsutake K, Ohara T, et al. Recent picture of infective endocarditis in Japan. Circ J Mar 23 2013;77(6):1158–64.
[2] Habib G, Hoen B, Tornos P, et al. ESC Committee for Practice Guidelines. Guidelines on the prevention, diagnosis, and treatment of infective endocarditis (new version 2009). Eur Heart J 2009;30:2369–413.
[3] Mylonakis E, Calderwood SB. Infective endocarditis in adults. N Engl J Med 2001;345:1318–30.
[4] Greub G, Lepidi H, Rovery C, et al. Diagnosis of infectious endocarditis in patients undergoing valve surgery. Am J Med 2005;118:230–8.
[5] Breitkopf C, Hammel D, Scheld HH, Peters G, Becker K. Impact of a molecular approach to improve the microbiological diagnosis of infective heart valve endocarditis. Circulation 2005;111:1415–21.
[6] Capobianchi MR, Giombini E, Rozera G. Next-generation sequencing technology in clinical virology. Clin Microbiol Infect 2013;19:15–22.
[7] Shah N, Tang H, Doak TG, Ye Y. Comparing bacterial communities inferred from16S rRNA gene sequencing and shotgun metagenomics. Pac Symp Biocomput 2011:165–1176.
[8] Do T, Gilbert SC, Klein J, Warren S, Wade WG, Beighton D. Clonal structure of *Streptococcus sanguinis* strains isolated from endocarditis cases and the oral cavity. Mol Oral Microbiol 2011;26:291–302.